Botswana water and surface energy balance research program Part 2 : Large scale soil moisture and passive microwaves

A.A. van de Griend
M. Owe
A.T.C. Chang

bcrs
BELEIDSCOMMISSIE REMOTE SENSING

Botswana water and surface energy balance research program
Part 2 : Large scale soil moisture and passive microwaves

A.A. van de Griend
Institute of Earth Sciences, Dept. of Hydrology, Vrije Universiteit Amsterdam, The Netherlands
M. Owe
A.T.C. Chang
NASA/Goddard Space Flight Center, Hydrological Sciences Branch, Greenbelt, MD, USA

bcrs project no. AO-4.4
bcrs report no. 91-38B

ISBN 90 5411 027 9

February 1992

This report describes a project which was carried out in the framework of the NRSP-1, under responsibility of the Netherlands Remote Sensing Board (BCRS).

CIP-GEGEVENS KONINKLIJKE BIBLIOTHEEK, DEN HAAG

Botswana

Botswana water and surface energy balance research program. - [Delft] : BCRS, Netherlands Remote Sensing Board
BCRS project no. AO-4.4, uitgevoerd in het kader van het NRSP-1, onder verantwoordelijkheid van de Beleidscommissie Remote Sensing (BCRS)
Pt. 2: Large scale soil moisture and passive microwaves / A.A. van de Griend, M. Owe, A.T. Chang. - Ill., fig., tab.
- (BCRS report ; 91-38B)
Met lit. opg.
ISBN 90-5411-027-9
Trefw.: energie ; Botswana ; onderzoek / remote sensing.

CONTENTS

LIST OF FIGURES

Fig. 14 Simulation of the vertical distribution of top soil moisture. For explanation see text.

Fig. 15 R^2-values of regression analyses between $\tau^*_{6.6}$ (derived from soil emissivity modeling and satellite observations) and NDVI, $\tau^*_{(pol.dif)}$ and $\tau^*_{(pol.rat)}$ for different values of the soil moisture distribution factor α.

Fig. 16 Time series of 6.6 GHz single scattering albedo and optical depth derived from satellite observed dual polarized brightness temperatures and simulated soil emissivities: 6.6 GHz (a), 37 GHz (b) together with NDVI (c).

Fig. 17 Time series of vegetation indices $\Delta T_{6.6}$, ΔT_{37} and NDVI, all derived from satellite signatures, and the time series of soil moisture.

Fig. 18 Scattergram of MPDI versus NDVI. Also the relationship reported by Becker and Choudhury is indicated.

Fig. 19 Simulation results from the synergistic approach with $\Gamma_{6.6}$ and $\omega = 0.093$:
- a. Scattergram of $\Gamma_{6.6}$ versus NDVI.
- b. Scattergram of satellite derived below canopy soil surface emissivity versus observed top soil moisture, using $\Gamma_{6.6} = f(NDVI)$.
- c. Scattergram of satellite derived below canopy soil surface emissivity versus observed top soil moisture, using $\Gamma_{6.6} = f(MPDI)$.

Fig. 20 Simulation results from the synergistic approach with $\Gamma^*_{6.6}$ and $\omega = 0$:
- a. Scattergram of $\Gamma^*_{6.6}$ versus NDVI.
- b. Scattergram of satellite derived below canopy soil surface emissivity versus observed top soil moisture, using $\Gamma^*_{6.6} = f(NDVI)$.

Fig. 21 Time series of satellite derived below canopy soil emissivity (below) and simulated soil emissivity using the radiative transfer model in combination with large scale observed soil moisture.

LIST OF TABLES

1. INTRODUCTION

1.1 The Botswana Water and Energy Balance Research Program

The Botswana Water and Energy Balance Research Program was conceived as a three year study of the moisture and energy exchanges in a semi-arid savanna environment. The program was initiated to study and evaluate the integrated use of multi-spectral satellite remote sensing for monitoring the hydrological status of the earth's surface. The program consisted of two major, mutually related components, i.e.:

1. A Surface Energy Balance Modeling Component, built around a extensive field campaign, and

2. A Passive Microwave Research Component, which consisted of a retrospective study of large scale soil moisture conditions and Nimbus/SMMR 6.6 GHz and 37 GHz microwave signatures.

The first part of the programme (BOTSWANA-1) ran officially from 1 January 1988 till 31 December 1990. The Dutch contribution was funded by the Netherlands Remote Sensing Board (BCRS). This report explains the integrated approach of both components in general and further summarizes the results of the activities performed within the Passive Microwave Research Component.

Remote sensing from space is playing an increasingly important role in large scale environmental studies, especially in those related to the exchange processes between the earth's surface and the atmosphere. Remote sensing from space helps to understand the complex large scale relationships between surface conditions and climate. Surface conditions are to a large extend determined by the partition of the sun's energy into the surface energy balance terms. The availability of surface moisture for evapotranspiration regulates this partition and therefore plays a key role in ecosystems dynamics.

The terms of the water balance in semi-arid regions can be monitored using different types of remotely sensed information from satellites. The complex physical processes involved, however, usually require a multi-sensor or a synergetic approach to identify individual parameters. In our approach we focused on the combination of (a) thermal infrared, (b) visible and near infrared (NIR), and (c) passive microwave remote sensing. Such an approach is expected to give better insight into the spatial and temporal varibility of soil moisture content and evapotranspiration at different scales, and therefore may contribute to the development of a multiscale monitoring system of the physical status of the earth's surface.

The terms of the surface energy balance may be modeled using thermal infrared surface temperature observations and large-scale, near-surface synoptic meteorological data. Application of thermal infrared remote sensing and inverse modelling then allows to estimate the evaporative conditions of the surface. The vegetation cover and green leaf biomass may be derived from visible and NIR signatures. Separately, the moisture status of the surface may be derived from passive microwave signatures. The latter, however, requires an estimate of the green leaf biomass or the vegetation water content in order to determine and model the influence of the vegetation on the microwave signal gathered from space. It is obvious that an integrated approach, which uses the different types of remotely sensed signatures together, has advantages over separate applications of each data type. This integrated approach is being applied to the semi-arid savanna regions of Botswana and emphasis has been placed on the following items:

(a) estimation of evapotranspiration and soil moisture content by surface energy balance modeling, using thermal infrared signatures and additional estimates of the vegetation characteristics such as leaf area index (LAI);

(b) estimation of the vegetation characteristics (such as green leaf biomass, water content and LAI), using visible and NIR signatures; and,

(c) estimation of soil moisture content in areas mainly covered with low natural savanna vegetation and intermixed with agricultural fields, using passive microwave signatures.

The basic structure of this integrated use of the different signals is shown in Fig. 1. This figure illustrates that the research items mentioned above are complementary in the sense that (b) gives important information to perform both (a) and (c), while (c) gives additional information to perform (a). The application of both microwave and thermal infrared methods requires some information on the vegetation and its structure. For passive microwave emission this is needed primarily to model or estimate the transfer of the signal through the canopy, whereas for thermal infrared it forms an integral part of the process of momentum, heat and moisture exchange within the earth-atmosphere interface. This explains the necessity to integrate vegetation information derived from visible and near-infrared data with both microwave and thermal-infrared remote sensing.

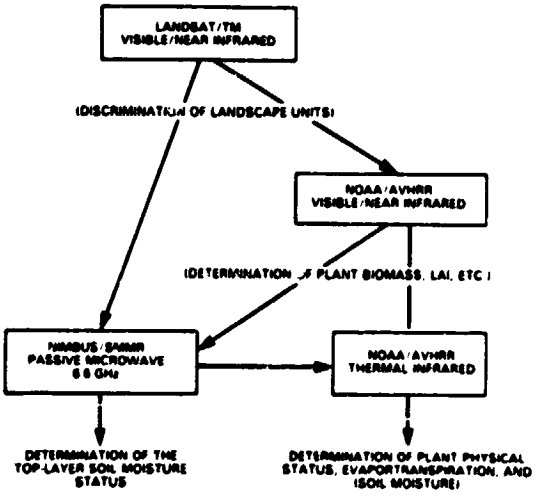

Fig. 1 Schematic representation of the integrated use of different types of remotely sensed signatures for monitoring the physical-hydrological status of the surface in (semi-)arid regions.

1.2 Large Scale Soil Moisture and Passive Microwaves

The relationship between the microwave emission of natural surfaces and their inherent moisture content has been studied and well-documented in the literature (Schmugge, 1985). This strong, physically based inverse relationship is due to the dielectric properties of soil and water mixtures, and lends itself well to satellite remote sensing techniques.

Reliable large-area soil moisture estimates are an essential element for regional and global water balance and climate-related studies. Remotely sensed surface moisture observations reflect areally integrated conditions, and therefore are more representative than averaged point measurements.

Most of the documented studies have depicted results of truck-mounted and aircraft radiometer experiments. These investigations have not only demonstrated the basic relationship between microwave emissivity and surface moisture, but have also helped to quantify the effects of various surface parameters, e.g. surface roughness and various vegetation aspects that distort and confound the basic relationship.

Investigations with satellite data have been fewer. However, the Scanning Multi-channel Microwave Radiometer (SMMR) on board Nimbus-7 has been used by several authors to study the relationship between microwave brightness temperatures and soil moisture (Wang, 1985; Choudhury and Golus, 1988; Owe et al., 1988). In the absence of large scale soil moisture observations, they all used some type of indicator for soil moisture conditions (such as API) and showed significant relationships with observed 6.6 GHz radiation.

The microwave emissivity of a complex vegetation covered surface is also determined by the radiative transfer characteristics of the vegetation cover (Jackson et al., 1982, 1990). The use of passive microwave to determine the moisture content of the top soil, therefore requires that the influence of the overlying vegetation is corrected for (Ulaby et al., 1983; Theis and Blanchard, 1988). The influence of the vegetation increases with increasing water content (Ulaby et al., 1986) and with increasing frequency. From the frequently used wavelength bands with frequencies of 1.5, 6.6 and 37 GHz, the 1.5 GHz (λ = 21 cm) is the most suitable for soil moisture monitoring (Schmugge, et al., 1986) due to the highest penetration depth of the soil and the highest capability to penetrate vegetation.

The radiative transfer characteristics, expressed in terms of the vegetation optical depth τ, are mainly determined by the vegetation water content (Ulaby, 1986). Theoretical and empirical models have shown the relationship between vegetation optical depth in the microwave region and vegetation water content (Mo et al., 1982; Ulaby et al., 1986; El-Rayes and Ulaby, 1987; Ulaby and El-Rayes, 1987). Water content is also related to green vegetation biomass and this has led to several empirical relationships between vegetation water content and NDVI (Tucker, et al., 1983; Kennedy, 1989). Verification of such theoretical and empirical relationships for satellite applications, however, is difficult because of the inherent large scale (> 100 km) for 6.6 GHz on Nimbus/SMMR, the inhomogeneity of the vegetation and the influence of spatially variable soil moisture.

The high spatial variability of surface moisture makes it an extremely difficult parameter to quantify on a regional scale, especially in remote, semi-arid environments where precipitation is also highly variable. This study is based on a large data base of surface soil moisture measurements, collected in three large experimental areas in the south-eastern part of Botswana (Fig. 2). These experimental areas

are approximately 20 km2 in size, and have over 50 soil sampling sites each. The study covered the period from October 1984 to July 1987.

In order to determine the effective optical depths of the vegetation at different microwave frequencies, we used a multi-layer radiative transfer model together with the dataset of large-scale and long-term soil moisture content. The major objectives of the study are:

(a) to quantify the relationship between satellite microwave measurements and surface moisture in a semi-arid savanna environment, using more accurate estimates of large-area soil moisture and vegetation characteristics; and,

(b) to use this information as a basis for inverse modeling of soil surface emissivity using a synergetic approach.

The microwave data are from the Scanning Multichannel Microwave Radiometer (SMMR) on-board the Nimbus-7 satellite. The resolution of the instrument is approximately 150 km at a frequency of 6.6 GHz (λ = 4.5 cm). The analysis of the relationships between Nimbus/SMMR 6.6 GHz passive microwaves and large scale soil moisture is decribed in Chapter 5. The inverse modeling approach is described in Chapter 6.

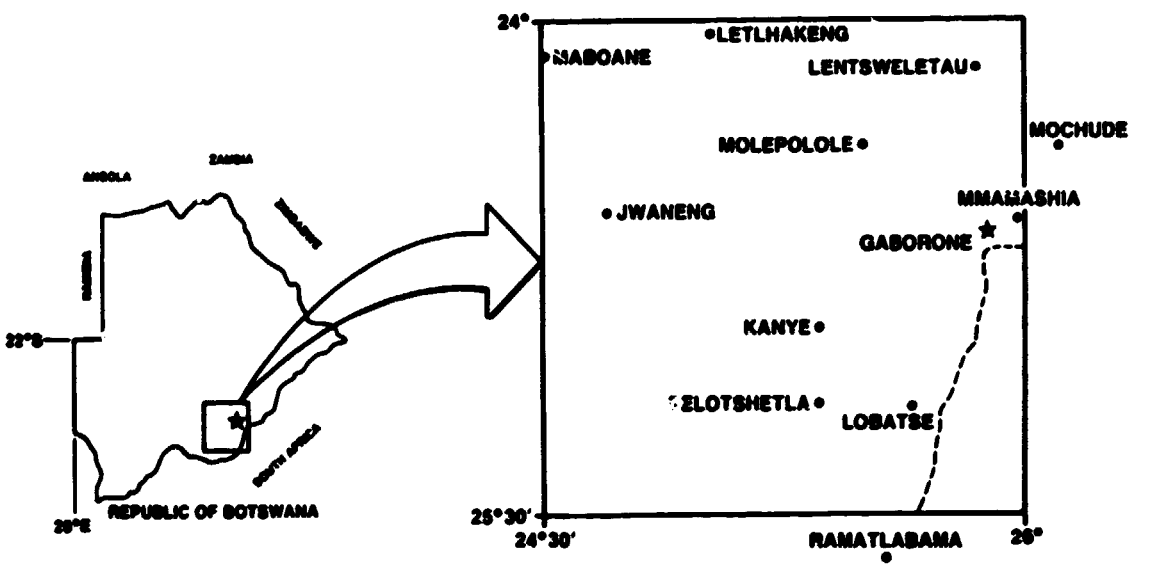

Fig. 2 Location of the 150 km square study area, including the distribution of climatic and data stations.

2. MICROWAVE THEORY

2.1 Soil Dielectric Constant

The utility of microwave radiometry in the sensing of surface moisture is based on the dielectric properties of soil-water mixtures and their effect on the emission of natural thermal radiation in the microwave region of the spectrum.

The dielectric constant, κ, is an electrical property of matter, and is a measure of the response of the medium to an applied electrical field. Its square root is the index of refraction of the medium. The parameter contains a real and an imaginary part (complex number), and as such is difficult to measure. In a non-homogeneous medium such as soil, κ is a combination of the dielectric constants of the individual constituents, i.e. air, water, rock, etc., and has led to the development of various mixing formulas (Wang and Schmugge, 1980; Wang, 1980; Jackson and O'Neill, 1986; Dobson et al., 1985).

In a soil medium, κ is largely a function of frequency, temperature, salinity and moisture content. At low frequencies, e.g. 1.4 GHz, the real part of k for water is approximately 80, while for a dry soil it is generally less than 5. A wet soil, therefore, may attain a value of 20 or more. Under ideal conditions, this difference causes a range of emissivities of about 0.95 for dry soil to less than 0.6 for wet soil (Schmugge, 1985; Wang and Schmugge, 1980). As the frequency increases, κ is seen to decrease, resulting in a decrease in the range of emissivity (and subsequently sensor sensitivity) from dry to wet soils.

To illustrate the behaviour of the dielectric constant for a range soil-water mixtures, typical of the moisture contents encountered in this study, we used an empirical dielectric mixing model (Wang and Schmugge, 1980). Table 1 contains the average soil physical characteristics in the study area. Soil characteristics used were representative of the soil conditions found in the study area (Botswana Ministry of Agriculture, 1985; Siderius, 1973). Both real and imaginary parts of the complex soil dielectric (for a frequency of 6.6 GHz) are illustrated in Fig. 3.

TABLE 1

TEXTURE(%)			VOLUMETRIC MOISTURE			
SAND	SILT	CLAY	WP	FC	BD	POROSITY
85	8	7	.05	.18	1.55	.42

SOIL MOISTURE VS. SOIL DIELECTRIC

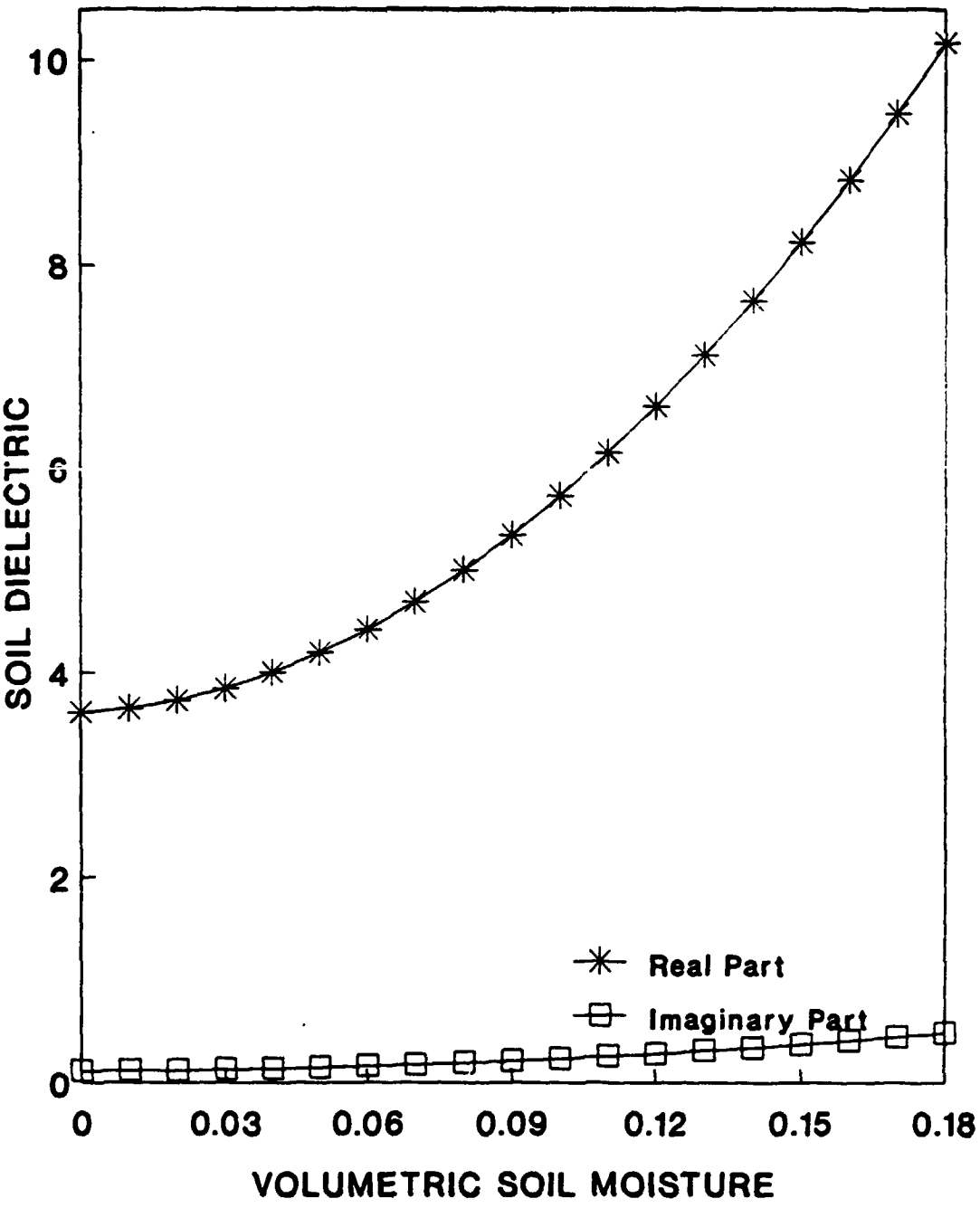

Fig. 3 The real and imaginary parts of the theoretical complex soil dielectric constant for the range of typical soil moistures encountered. Values were derived using the model from Wang and Schmugge (1980) for representative soil conditions in the study area at a frequency of 6.6 GHz.

2.2 Emissivity

For a thick dielectric medium, the sum of its reflectivity (R) and absorptivity (A) must equal one. It follows, then, that for a non transmitting medium, the emissivity (ε) will be given by

$$\varepsilon = 1 - R \qquad (1)$$

Theoretical horizontally polarized reflectivity was calculated from the corresponding Fresnel equations (Schmugge, 1985), using the previously computed values of κ and the SMMR look angle of 50°. Although the emissivity in the vertical polarization is considerably higher than the horizontal, the dynamic range for corresponding soil moistures is much less. This makes horizontally polarized data much more useful.

In addition to soil moisture content, microwave emission is dependent on a series of other surface characteristics such as vegetation cover, surface roughness and other factors as indicated in Fig. 4. These influences have been well documented in past research activities (see e.g. Jackson et al., 1982; Schmugge et al., 1986; Jackson and O'Neill, 1990).

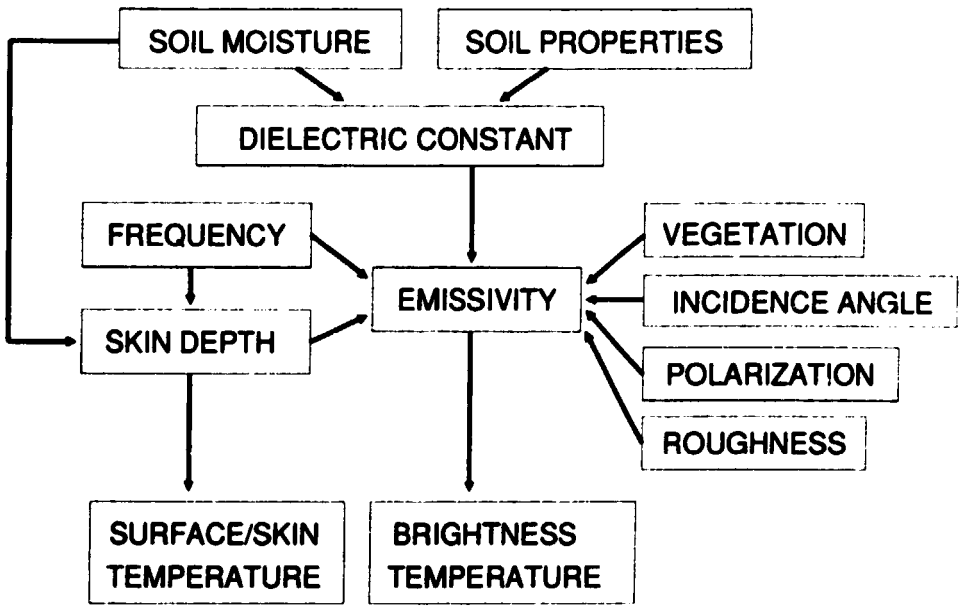

Fig. 4 Factors influencing the emissivity of a complex vegetation covered surface.

2.3 Soil Roughness Effects

Surface roughness causes the emissivity of natural surfaces to be somewhat higher (Schmugge, 1985). This is attributed primarily to the increased surface area of the emitting surface. In addition, the dynamic range (from wet soil to dry soil) decreases as the surface roughness increases (Wang, 1983). For example, the difference in brightness temperature between wet and dry soil conditions was found to be approximately 120 K for a smooth surface, 80 K for a surface with medium roughness, and only 40 K for a rough surface (Schmugge, 1985). Theis et al. (1986) found that incorporating a surface roughness parameter derived from an active microwave response (radar) significantly improved the observed relationship between soil moisture and microwave brightness temperature.

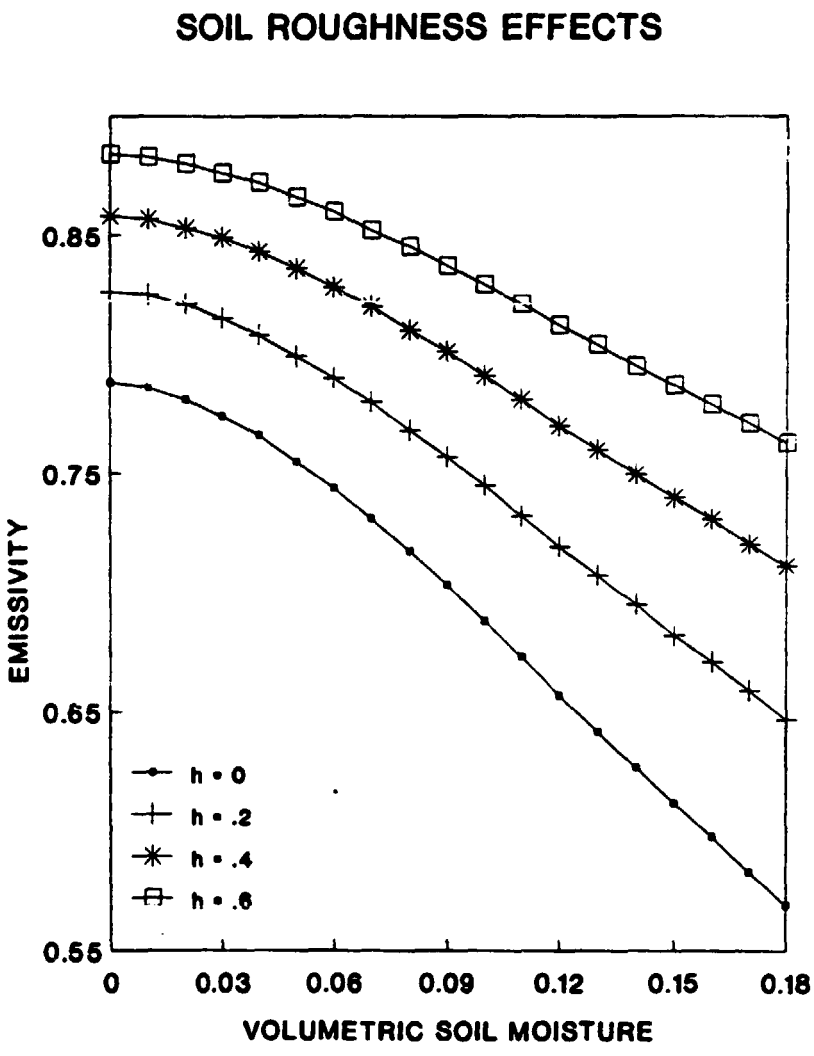

Fig. 5 Relationship between soil moisture and the theoretical emissivity for a range of surface roughnesses, using the roughness parameter of Choudhury et al. (1979).

To demonstrate the effects of surface roughness, an empirical roughness model (Choudhury et al., 1979) was applied to the theoretical surface emissivities calculated previously. The rough bare soil emissivity (ε_s) may be calculated as

$$\varepsilon_s = 1 - R^* \exp(-h\cos^2 u) \qquad (2)$$

where h is a dimensionless empirical roughness parameter. Choudhury et al. (1979) listed some typical values of h and their corresponding surface conditions as 0 (smooth surface), 0.3 (disced field), and 0.5 (rough plowed). Wang (1983) determined that the incidence angle dependence of the correction factor for h was not strong, and based on data, recommended deleting the $\cos^2 u$ term, which in this case was done. The relationship between emissivity and surface moisture for a range of surface roughness values is illustrated in Figure 5.

2.4 Vegetation Effects

The effects of vegetation on the microwave emission measured above the canopy are two-fold. Vegetation may absorb or scatter radiation eminating from the soil, and will also emit radiation itself. In areas of sufficiently dense vegetation, the emissivity measured above the canopy may be due entirely to the vegetation.

Numerous canopy models have been developed and used to account for the effects of the vegetation (Kirdiashev et al., 1979; Mo et al., 1982; Theis et al., 1984; Ulaby et al., 1986). These basic models have been modified and applied successfully by a variety of researchers using primarily truck-mounted radiometer data over agricultural fields (Jackson et al., 1982; Pampaloni and Paloscia, 1986; Jackson and O'Neill, 1990).

A formulation given by Ulaby et al. (1986), among others, for a uniform canopy layer was used. Assuming similar soil and canopy temperatures,

$$\varepsilon_c = (1 + (1 - \varepsilon_s)\Gamma)(1 - \Gamma)(1 - \alpha) + \varepsilon_s\Gamma \qquad (3a)$$

or $$\varepsilon_c = 1 - (1 - \varepsilon_s)\Gamma^2 \quad (\text{when } a = 0) \qquad (3b)$$

where ε_c is the emissivity measured above the canopy, α is the single scattering albedo, and S is the one-way transmissivity. The transmissivity is the ratio of the radiant energy transmitted through a medium to that incident upon it, and may be expressed as a function of the optical depth τ and the incidence angle in the following manner:

$$\Gamma = \exp(-\tau/\cos u) \qquad (4)$$

2.5 Optical Depth

Optical depth is related to the canopy density, and also has been shown to be a linear function of vegetation water content. Typical values of s for agricultural crops have generally been given as less than

OPTICAL DEPTH EFFECTS

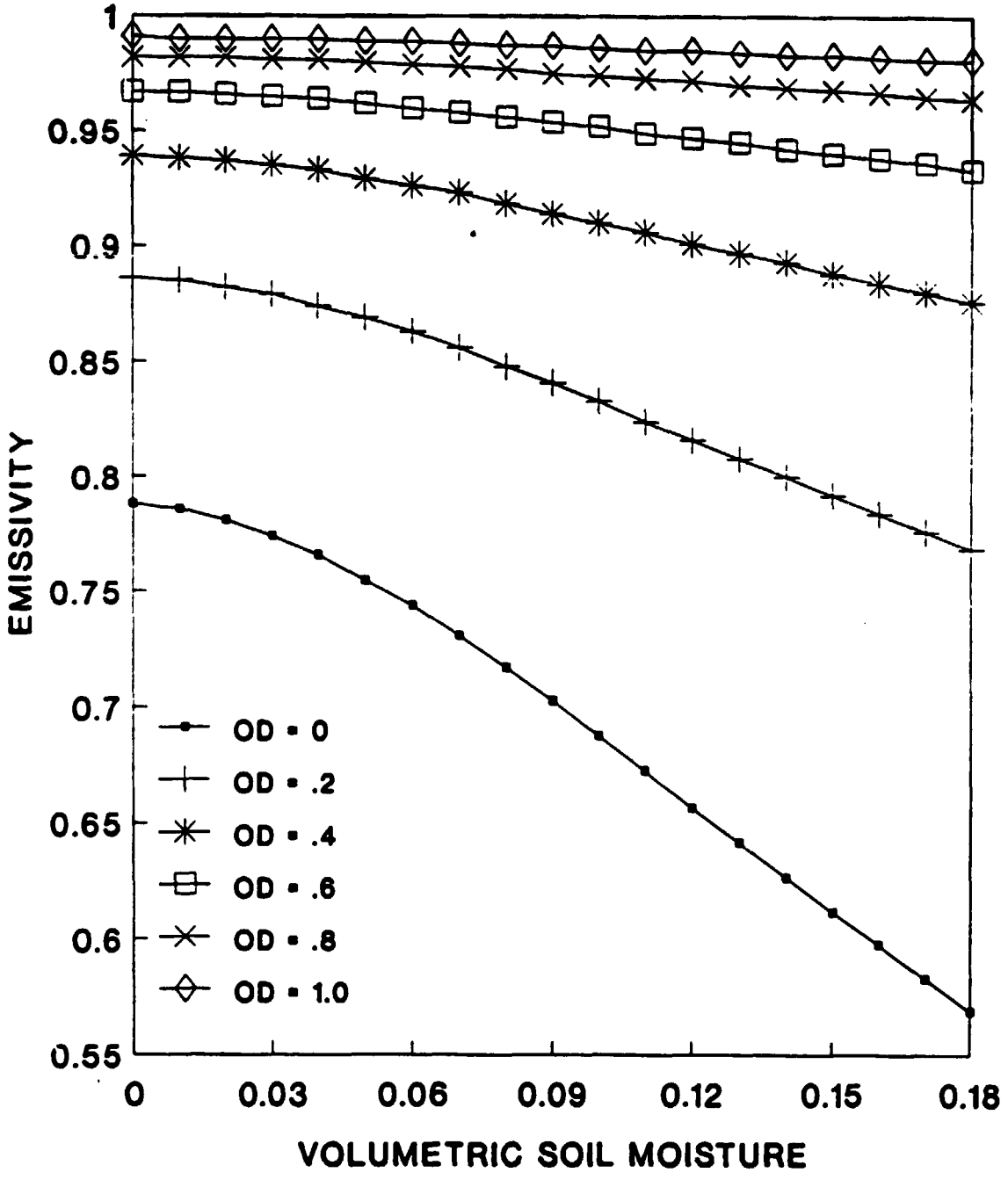

Fig. 6 Relationship between the theoretical above-canopy emissivity and soil moisture for a range of optical depths.

one (Mo, et al., 1982; Jackson and O'Neill, 1990). Theoretical calculations (Ulaby et al. 1986) have shown that the sensitivity of the above-canopy brightness temperature (T_b) measurements to variations in soil emissivity decreases with increasing optical thickness. The effective T_b range between dry (5% moisture) and wet (35%) soils is shown to be about 100 K and 15 K at optical depths of 0 and 1 respectively.

Using the above vegetation model [3a], the theoretical above-canopy emissivity was calculated for a range of optical depths (with h = 0). It is seen in Figure 6 that the emissivity increases with optical depth, whereas the dynamic range of ε from a dry to a wet surface decreases. This is because the emission from the vegetation tends to saturate the signal with increased optical depth. The net result is a decrease in sensor sensitivity to soil moisture variations.

2.6 Single Scattering Albedo

One may expect the albedo, α, to be a function of individual plant geometry, polarization, and frequency, and consequently should vary with species, plant associations and vegetation density. The single scattering albedo describes the scattering by the vegetation of the upwelling radiation from the soil. Experimental data for for this parameter are limited, and values for selected crops vary from 0.04 to about 0.12 (Brunfeldt and Ulaby, 1984; Jackson and O'Neill, 1990). Simply setting $\alpha = 0$ is also quite common. Experimental values for the single scattering albedo for natural vegetation surfaces are even less common.

The effects of the single scattering albedo on the theoretical bare soil emissivity do not appear to be great at either the spatial scale used here or average vegetation densities typically found in this type environment (i.e., $\alpha < 0.05$ and $\tau < 0.25$). While the observed emissivity does decrease with increasing a, theoretical calculations have shown less of an effect on the dynamic range of ε from dry to wet soil conditions. Illustrations of the single scattering albedo effects may be found in Fung and Eom (1985) and Ulaby et al. (1986).

2.7 Wavelength Effects

The effect of wavelength is such that an increase in k provides better "penetration" of the surface, or more accurately, the source of the emission lies deeper within the soil and thus is more representative of a deeper soil temperature. The effective penetration depth also depends on soil moisture, but will seldom vary more than several tenths of a wavelength under any condition (Ulaby et al., 1986). Moreover, this relationship is only slightly dependent on soil type at 6.6 GHz. In addition, longer wavelengths are better able to penetrate vegetation canopies. An optimum wavelength for soil moisture remote sensing has been shown to be about 21 cm (Schmugge, 1985).

3. STUDY SITE AND DATA DESCRIPTION

3.1 Site Characteristics

The study area is approximately 150 km square in south central Botswana (Figure 2), and corresponds nominally to a SMMR footprint. The southeast edge of the region has some low hills along

the South African border, and while some of the area may be slightly undulating in places, it is for the most part relatively flat.

Most of the region may be classified as tree and shrub/grass savanna, and is often interspersed with cultivated fields in many areas. In some areas, the existing cover is nothing more than sparse grasses, while much is also bare. Relatively dense woodland may be found on some of the better soils along drainages, where trees may average 6 - 10 meters in height, and will occassionally attain heights of 12 meters or more. Much of the area is used as open range. Vegetation density tends to decrease from SE to N and W, in response to precipitation gradients. The northern edge of the study site is at the southern fringe of the Kalahari Desert. Excellent descriptions of the vegetation, topography and land use character of the region are given by Ringrose and Matheson (1987) and Ringrose et al. (1990a; 1990b).

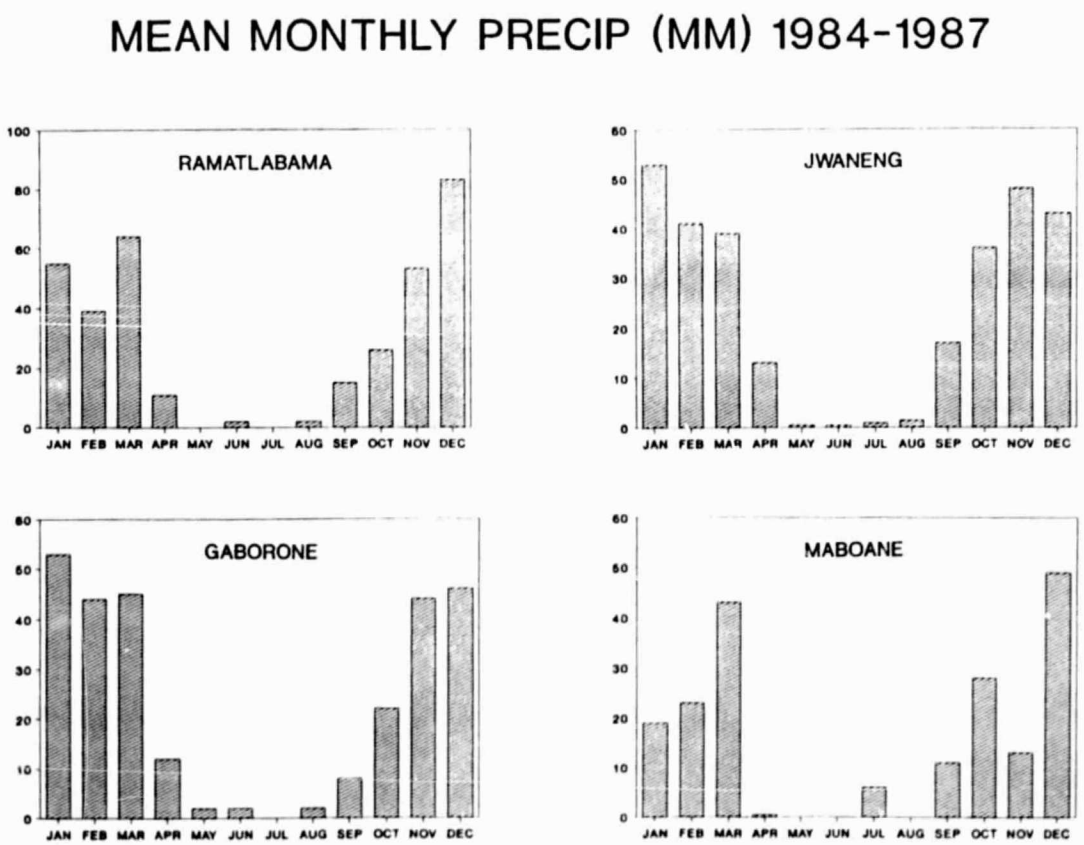

Fig. 7 Mean monthly precipitation during the study period for several stations within the test area.

Botswana is characterized as semiarid, with hot, relatively moist summers and cool dry winters. The mean daily air temperature during the summer and winter is approximately 25°C and 17°C respectively. Precipitation is highly variable in both time and space throughout the region and varies from about 300 mm annually in the West to almost 500 mm in the East. Mean monthly precipitation during the study period is shown for several stations (Fig. 7).

3.2 Data

The soil moisture data used in this study were collected in three experimental areas; Pelotshetla in the south of the footprint, Sebele, slightly north of Gaborone, and Oodi-Mmamashia to the east of Sebele. Soil moisture data were collected every 7 to 10 days during the growing season, in vertical profiles by neutron probe. We used the upper-most measurements which were representative of the top 20 cm of the profile. Each experimental area consisted of numerous fields with different surface covers, i.e. natural bare (uncultivated) soil, natural savanna grass and bush, and agricultural fields with a variety of crop covers and cultivation practices. In each experimental area about 50 to 60 neutron probe access tubes were monitored. Daily precipitation data from 12 stations located within the study area were also used (Fig. 2). Daily minimum and maximum temperatures and solar radiation were recorded at two locations. Remotely sensed data included 6.6 GHz (k = 4.5 cm) SMMR brightness temperature (T_b) measurements and monthly composites of the Normalized Difference Vegetation Index (NDVI) calculated from visible and near infrared reflectances as measured by the Advanced Very High Resolution Radiometer (AVHRR) on the NOAA-9 satellite in a manner similar to Tucker et al. (1984). Land use character assessments of the overall study area were made from Landsat-5 Thematic Mapper and SPOT images.

4. ANALYSIS OF BOTSWANA DATA

4.1 Areally Averaged Soil Moisture

Although several studies relating satellite passive microwave data to surface moisture may be found in the literature (Wang, 1985; Choudhury et al., 1989; Owe et al., 1988), none have used actual large area average soil moisture data. Past studies have used only daily antecedent moisture index data, calculated from simple empirical API models based on limited climatic data, usually precipitation and temperature. Although these techniques may give some indication of relative day to day surface wetness, they bear little resemblance to actual daily surface moisture values. In addition, the high spatial variability of surface moisture makes it an extremely difficult parameter to quantify accurately, especially in remote, semi-arid and other moisture limiting regions where precipitation characteristics are also highly variable.

As mentioned earlier, this study is based on a large number of long-term soil moisture measurements, taken at 7 to 10 day intervals, in different experimental fields located within the 150 km study area. Because the soil moisture measuring days do not generally coincide with a SMMR overpass, we had to model surface soil moisture on a daily basis. For this purpose we used a physically based technique that has been shown to successfully replicate daily soil moisture in the surface profile by using the actual field measurements to calibrate the model (Owe and Van de Griend, 1990).

Although the model has been shown to provide highly reliable estimates of actual surface moisture on a field basis, good spatially representative precipitation measurements remain the most limiting factor for determining large area averages. It is felt that the data available for this study provided the representative coverage necessary for achieving accurate large area estimates. The moisture model and modelling results for the different land covers will be discussed next.

4.2 Surface Moisture Model

Daily surface soil moisture is modelled in a manner similar to Owe and Van de Griend (1990). The change in daily surface soil moisture is given by the simple continuity equation

$$\frac{d\theta}{dt} = -ET + P \qquad (5)$$

where θ is the moisture content of the 20 cm surface profile (mm), t is the time interval (days), P is the daily precipitation (mm) and ET is the daily evapotranspiration (mm). The evapotranspiration is calculated using a modified Priestley and Taylor (1972) model, and is given by

$$ET = \beta \frac{D}{L(\Delta+\gamma)} (R_n - G) \qquad (6)$$

where R_n is the net radiation, G is the soil heat, L is the latent heat, Δ is the slope of the temperature/saturated vapor pressure curve, γ is the psychrometer constant and β is an empirical coefficient which describing the evaporation, and is a function of soil moisture.

The soil heat is often a difficult parameter to estimate. It may be parameterized as a simple fraction of the net radiation, based on the character of the surface (Brutsaert, 1982). Choudhury et al., (1987) describe G as an exponential function of the leaf area index for vegetated surfaces, but it was found (Owe and Van de Griend, 1990) that

$$G = [0.266 - 0.197 \exp(-6.39(1-\theta_{fc}))] R_n \qquad (7)$$

where θ_{fc} is the moisture content of the surface 20 cm profile expressed as a fraction of the field capacity described this relationship reasonably well under bare conditions.

It has been shown that the β term does not always equal 1.26 as proposed by Priestley and Taylor (1972), not even for surfaces transpiring at the potential rate, but is is strongly related to the surface condition, soil physical properties and to the relative moisture content (Davies and Allen, 1973; De Bruin,

TABLE 2: Modelling results for different surface characteristics at the three experimental sites, using the approach described in Owe and Van de Griend (1990).

EXPERIMENTAL SITE	LAND COVER	RESIDUAL MEAN SQUARE2
Oodi-Mmamashia	Cultivated	6.1
	Bare	6.5
	Grass/Shrub	4.8
Sebele	Cultivated	4.1
	Grass/Shrub	6.5
Pelotshetla	Cultivated	4.3
	Grass/Shrub	4.3

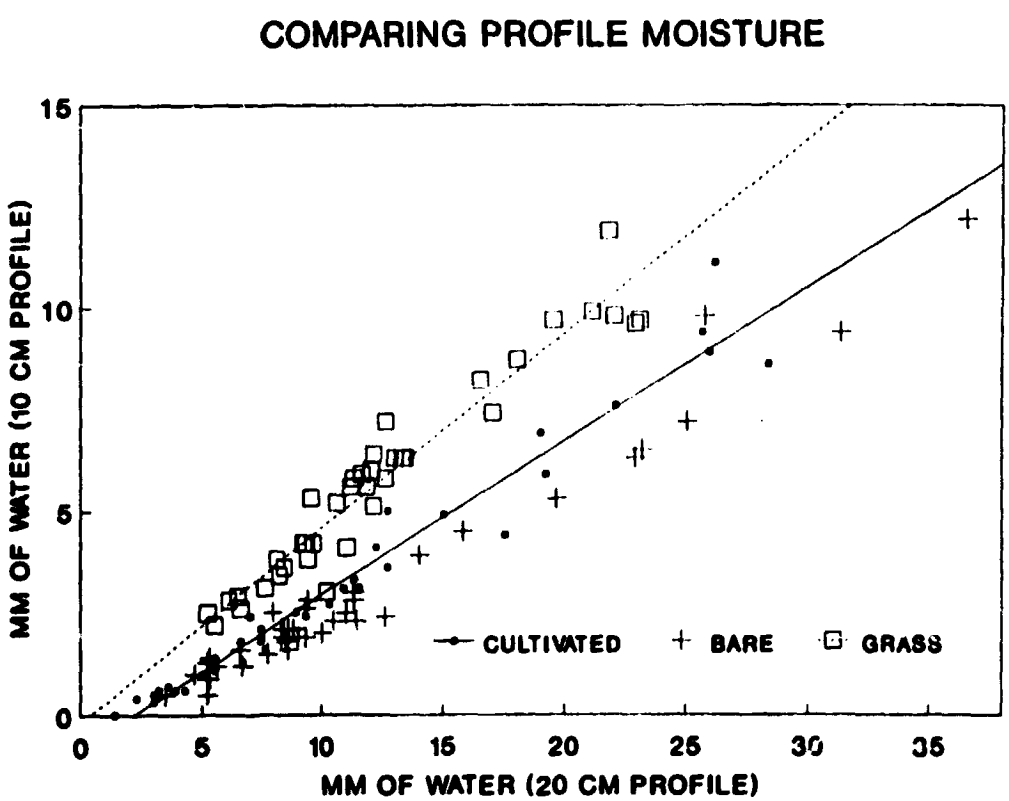

Fig. 8 Comparison between moisture contents measured in the 10 cm and 20 cm surface profiles. These relationships were used to convert the 20 cm profile data to 10 cm data for the various surface covers (1983).

It has been shown (Owe and Van de Griend, 1990) that the evaporative coefficient may be described by

$$\beta = a + b \exp(c\theta_c) \qquad (8)$$

where a, b and c are empirical fitting parameters.

With this model all the soil moisture time series were modelled and then used to extract topsoil moisture for the days of satellite coverage.

4.3 Daily Average Footprint Surface Moisture

The average daily footprint soil moisture for the study site was calculated using a simple partial area concept. The reliability of regional soil moisture estimation is largely a function of the spatial distribution of the precipitation data. Therefore, data from 12 precipitation stations were used. The 1.5° square study site was partitioned around the precipitation stations by a Thiessen Polygon network (Bruce and Clark, 1966), and the corresponding weights calculated for each. Within each of the polygons, the percent area in each of three cover types; bush/grass savanna, cultivated and bare, was estimated from Landsat TM and SPOT-MSS scenes.

This represented the full range of cover types found in the region. As described earlier, soil moisture was measured within each of these cover types at all three monitoring sites. Between 15 and 20 replications were made for each cover condition at each field site. Moisture content in the top 20 cm was reported for all sites, while some top 10 cm data were also reported.

The above-described moisture model was calibrated with the 20 cm data for each of the 3 cover types for each location. The time series were modelled with RMS values ranging from 4.1 to 6.5 (see Table 2). Simulations for each cover type were subsequently run for all the polygons with their corresponding precipitation data. All runs were made for a 20 cm profile, and then converted to a 10 cm profile based on the relationships in Figure 8. This step was performed because 10 cm soil moisture is more representative of what the satellite actually sees, although in reality, this too is somewhat optimistic. All daily values were then weighted according to cover type distribution within each polygon to obtain an average daily polygon surface moisture. These values were then weighted according to their respective polygon areas and then summed to arrive at the mean daily footprint surface moisture. The time series of pixel average top soil moisture is shown in Fig. 9.

5 RELATION BETWEEN OBSERVED LARGE SCALE SOILMOISTURE AND NORMALIZED BRIGHTNESS TEMPERATURES

5.1 Night-time Brightness Temperatures

The microwave emissivity of the surface may be estimated from the relationship

$$\varepsilon = \frac{T_b}{T_s} \qquad (9)$$

where T_s is the physical surface temperature and T_b is the microwave brightness temperature. We used nighttime 6.6 GHz microwave brightness temperatures. Because remotely sensed surface temperatures were not available, we normalized the microwave data by dividing T_b by the nighttime air temperature. Nighttime air temperature at the time of the satellite overpass (approximately 2300 hours) was approximated in the following manner,

$$T_a = (T_{max} + 2T_{min})/3$$

where T_{max} is the current day's maximum air temperature and T_{min} is the minimum air temperature of the following day, which generally occurs immediately prior to sunrise. This relationship was derived by analyzing several days of continuous diurnal temperature data.

During the daytime, the soil surface temperature heats up very quickly, and consequently, the surface skin layer becomes extremely dry, regardless of the average moisture content of the 20 cm surface profile. As a result of this steep gradient, the surface skin layer no longer bears any relationship to the profile moisture. At night, moisture moves upward as the profile approaches some equilibrium, and the skin layer is again wetted to some degree. Another advantage of nighttime data is that air temperature more closely resembles both the surface and the canopy temperatures at this time. Dew formation is generally not a problem at this hour.

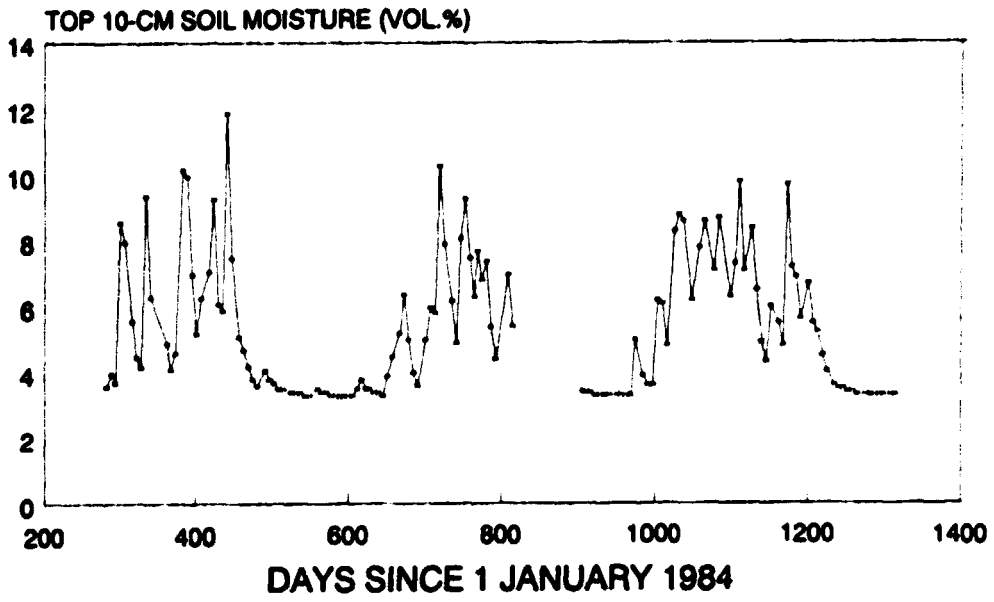

Fig. 9 The course of pixel average top soil moisture for the days of Nimbus/SMMR overpass, estimated from actually observed soil moisture data and using a daily soil moisture model for interpolation.

TABLE 3: Statistical data for satellite emissivity and soil moisture when data is grouped by NDVI range.

TREND LINE PARAMETERS AND STATISTICS

NDVI

Range	Slope	Intercept	n	r2
<.12	.48	.46	33	.69
.12-.20	.86	.79	69	.76
>.2	.63	.61	38	.47

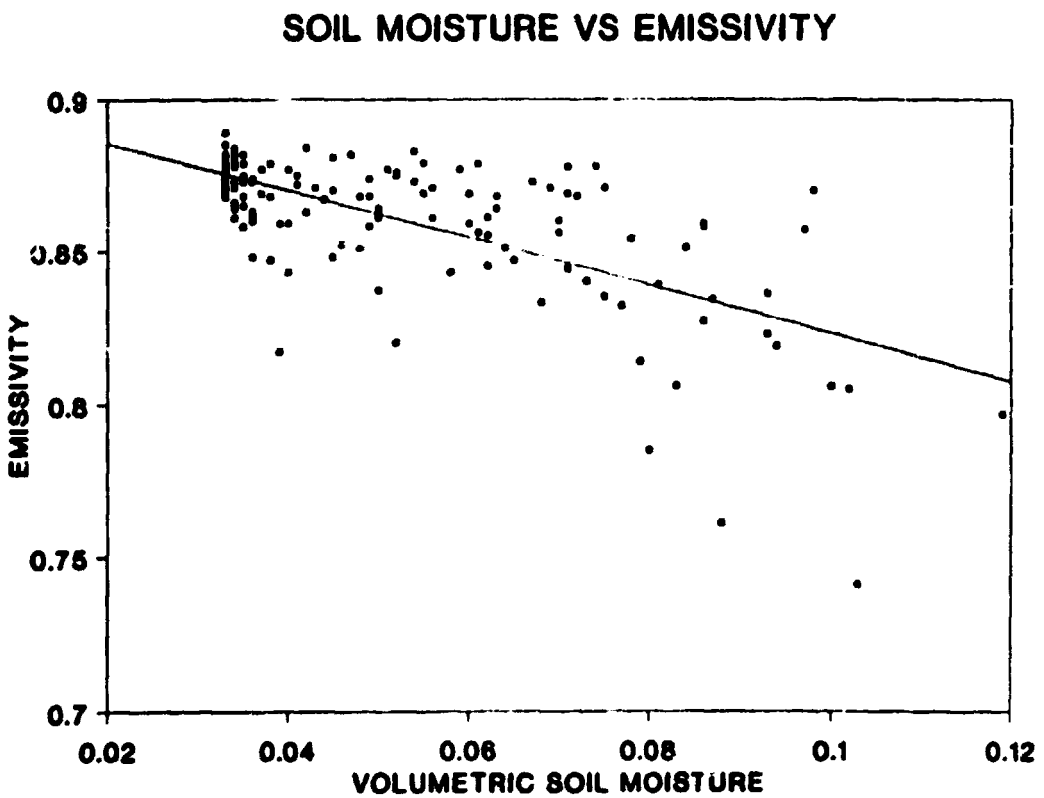

Fig. 10 The relationship between pixel average surface soil moisture and the above canopy emissivity as measured by Nimbus/SMMR; r2 = 0.45, n = 140.

5.2 Nighttime Brightness Temperatures and Footprint Soil Moisture

The nighttime normalized T_b values were compared with the footprint average daily soil moisture values. Initially, daytime SMMR data were used, but a much weaker relationship was detected. The nighttime data resulted in a significant but weak relationship with an explained variance (R^2) of 0.45. One should note, though, that the dynamic range of observed footprint average soil moisture values is, almost by definition, small, due to the large foot print.

The data were subsequently partitioned into seasonal time periods, which improved the relationship between emissivity and surface moisture significantly. The most variable parameter affecting the microwave emissivity in addition to soil moisture is the vegetation. Vegetation in semi-arid regions exhibits a high degree of seasonality which affects the remotely sensed emission in a non-uniform manner. A model which accounts for vegetation would normalize these seasonally variable effects. The NDVI provides an objective measure of the vegetation. We therefore grouped the data by NDVI range, and found significantly improved relationships for the subgroups (Table 3).

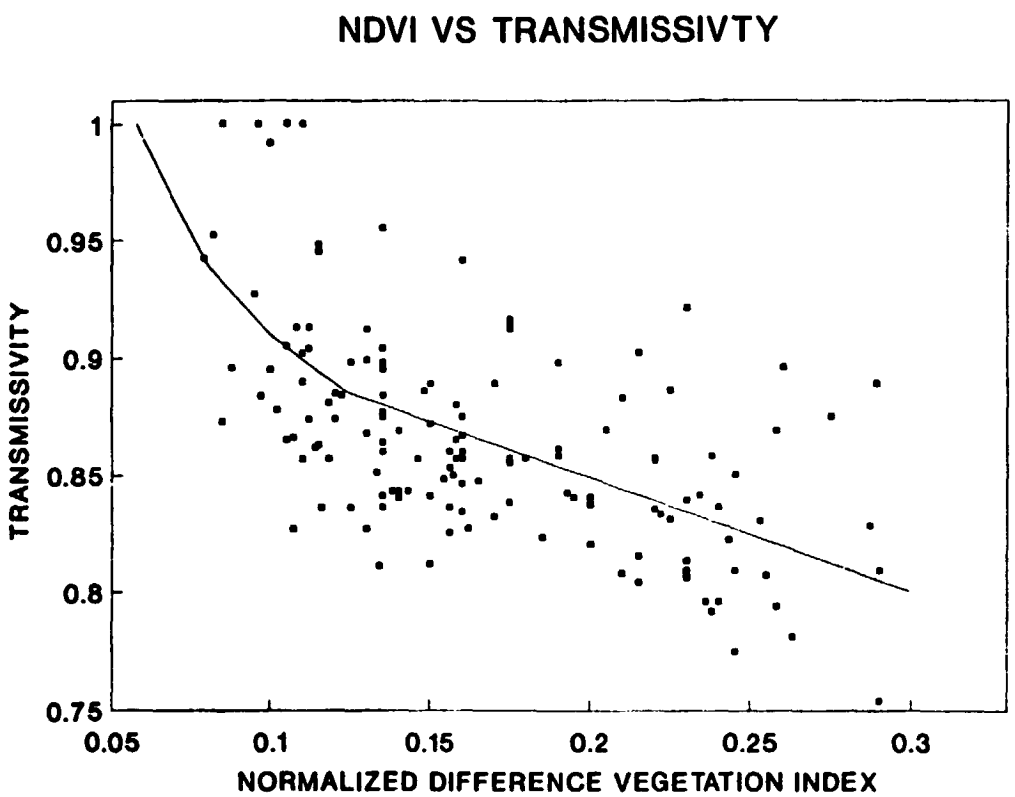

Fig. 11 Relationship between NDVI and the transmissivity. The data are best described (r = .61) by a two-part function; S = .945 - .48*NDVI when NDVI>.123 and S = .945*exp(-17.1*NDVI) + .827 when NDVI<.123.

5.3 Vegetation Influences

Assuming a zero single scattering albedo and solving eq. [3] for the transmissivity, we get

$$\Gamma = \left[\frac{\varepsilon_c - 1}{\varepsilon_s - 1}\right]^{1/2} \qquad (10)$$

where ε_s is the satellite observed emissivity from Figure 10, and ε_c is the calculated theoretical bare soil (h = 0.3) emissivity based on the actual daily surface moisture. The roughness parameter of 0.3 corresponds to a medium rough surface (Choudhury et al., 1979), and would appear reasonable for an average footprint condition. Figure 11, relates the NDVI to the transmissivity, and although the correlation is weak, a trend does exist. The NDVI values have been interpolated from monthly Global Area Coverage (GAC) composites (Tucker et al., 1985). These data reflect only the general seasonal trend, and no longer reflect any short term variability due to greening from individual precipitation events. Daily or 7 to 10 day composite NDVI data may improve this relationship, although the possibility of cloud contamination is greatly increased.

Indices such as the NDVI are often used to quantify vegetation parameters, and have been used successfully to monitor and study vegetation trends on regional, continental and global scales (Tucker et al., 1984; 1985). Channel 1 measures the reflectivity in the visible spectrum while Channel 2 measures the reflectivity in the near infrared. The success of this technique is due to the differential reflectance of green leaf chlorophyll at these two wavelength bands. Green vegetation will normally have a reflectance of less than 20% in the visible, and as much as 60% in the near IR. The NDVI, which is expressed as

$$NDVI = \frac{Ch2 - Ch1}{Ch2 + Ch1} \qquad (11)$$

is then essentially a measure of the greenness of the vegetation, and hence an indicator of and related to total green leaf biomass and leaf area.

The variability of the NDVI at low levels of vegetation due to soil color and other factors has been shown (Ringrose and Matheson, 1987). Therefore it may not be the most reliable indicator of total vegetation biomass under these conditions. This may be true especially during periods of dormancy, when large amounts of woody plant material are still present, but have little effect on the greenness index. Although vegetation water content is an important factor in microwave attenuation, woody plant material and senesced vegetation may also be of influence. This aspect must be studied further because of the relatively high ratio of woody and dead plant material to green leaf material in semi-arid areas.

Not withstanding the shortcomings of the NDVI as a vegetation parameterization, we used the relationship shown in Figure 11 to estimate the transmissivity. Using the satellite derived emissivity, ε_s, along with the estimated transmissivity function, and reinserting them into eq. [3], we now solved for the corrected bare soil emissivity, ε_c, and compared these values (Fig. 12) to the previously calculated theoretical soil emissivities based on the footprint average daily surface moisture. Although a one to one correspondence along the line x=y would be ideal, it is seen that the corrected satellite emissivities are underestimated at the lower values and slightly overestimated at higher values.

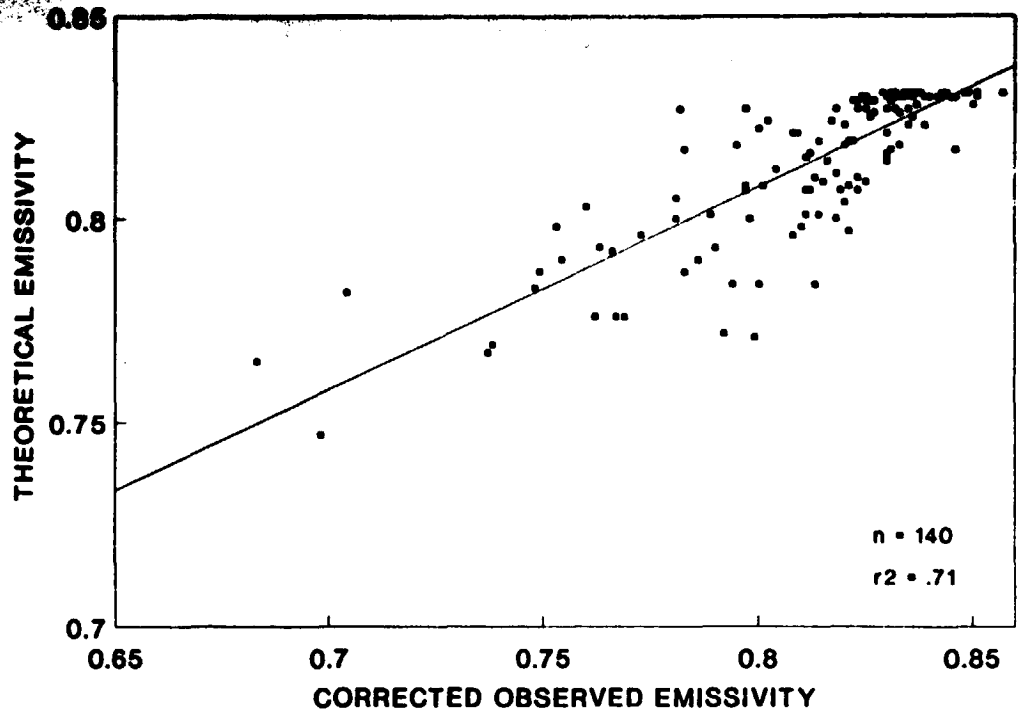

Fig. 12 The vegetation-corrected satellite emissivity is plotted against the theoretical bare soil emissivity. Although, ideally, the regression should be close to the x = y line, the compositing procedure and the monthly parameterization of vegetation will undoubtedly introduce a bias when applied to instantaneous values of satellite microwave emissivity.

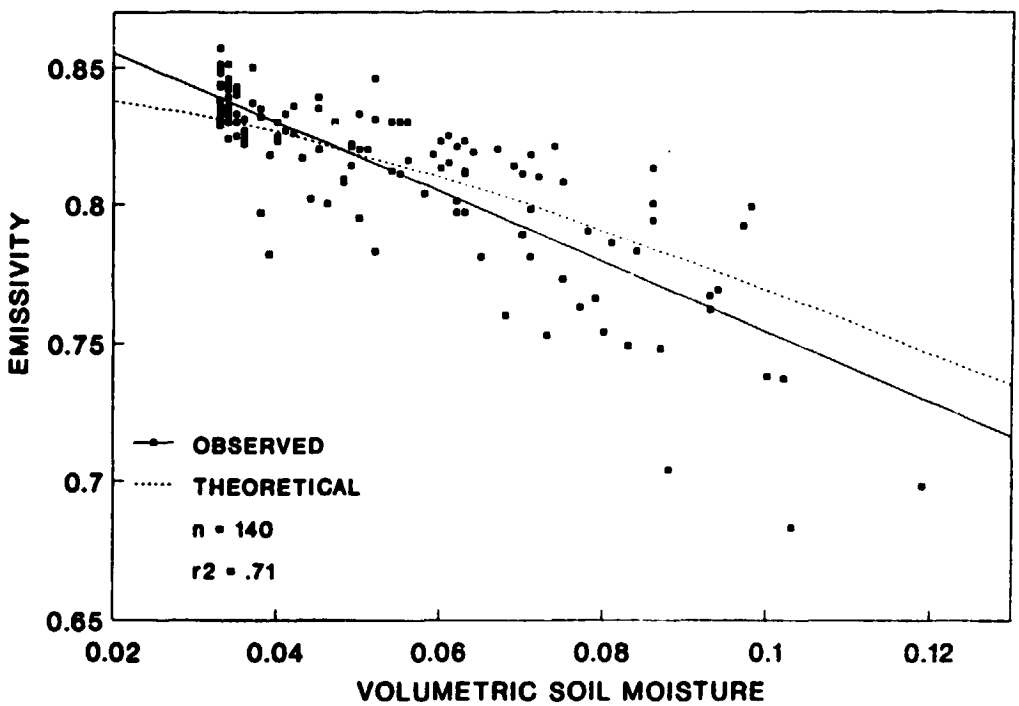

Fig. 13 Soil moisture vs the vegetation-corrected satellite emissivity. Also plotted for the purpose of comparison is the theoretical bare soil emissivity.

The NDVI appears to overestimate the vegetation effects during the wet season relative to the dry season. The excessive scatter may also be due to an inability of the NDVI to accurately parameterize the effect of the vegetation biomass during periods of low canopy density. The structure and composition of semi-arid (i.e. savanna) vegetation is such that there is a much greater ratio of woody plant mass to green leaf biomass than one generally finds in more temperate areas. Becker and Choudhury (1988) have indicated that the sensitivity of the NDVI decreases below a certain threshhold, which probably varies somewhat depending on the physical structure of the predominant vegetation. They also showed an improved sensitivity of the 37 GHz polarization difference to variations in vegetation biomass in this range. Additionally, monthly composite data does not account for variability in the vegetation during the month.

The corrected satellite emissivities are also plotted against the surface soil moisture (Figure 13). The high scatter previously observed is still somewhat noticeable, but now with a correlation coefficient of 0.84, and 71 percent of the variability in surface moisture accounted for. Also indicated in this figure is the line describing the theoretical soil emissivity for the range of moistures encountered, illustrating the ideal relationship. Regarding the fact that (1) the soil moisture ranges encountered for the 150 km square footprint are by definition in the dry region, (2) the estimation of footprint average soil moisture is extremely difficult even in this case with a tremendous amount of surface data, and (3) the fact that monthly composite NDVI values were used to estimate the transmissivity, the relationship found between footprint average soil moisture and vegetation corrected emissivity is surprisingly high. The analysis also demonstrates the necessity to correct for vegetation influences and addresses the necessity to approach soil moisture monitoring by a multispectral approach consisting of microwave, visible, near infrared remote sensing. Satellite derived thermal infrared data would also contribute significantly in estimating actual surface temperature.

6 VEGETATION CHARACTERISTICS AND INVERSE MODELING OF SOIL EMISSIVITY

6.1 Determination of Single Scattering Albedo and Optical depth

In order to estimate both the single scattering albedo and the large scale "effective" optical depth of the vegetation at 6.6 GHz and 37 GHz we applied a radiative transfer model. Knowledge of the vegetation optical depth is important for satellite-based large scale soil moisture monitoring using passive microwaves. The derived optical depths have been compared with microwave polarization differences and polarization ratio's in both frequences and with NDVI-values from NOAA/AVHRR. This formed the basis for a synergetic approach to derive surface soil emissivity from satellite observed brightness temperatures by inverse modelling. This approach also improves the relationship between satellite derived surface emissivity and large scale top soil moisture from R^2=0.45 (no correction for vegetation) to R^2=0.72 (after correction for vegetation). The analyses also confirm the relationship between the microwave based MPDI and NDVI earlier described and explained in the literature.

6.2 Soil Emissivity and Radiative Transfer Model

<u>Modelling of Soil Dielectric Properties</u>

Soil dielectric properties were modeled using a dielectric mixing model by Dobson et al. (1985) which describes the complex dielectric constant of the soil-water mixture. It requires only easily obtainable soil physical parameters, such as volumetric moisture and textural composition. This model, although semi-empirical, has been demonstrated to yield an excellent fit to experimental data at frequencies above 4 GHz. The model distinguishes between free water and bound water, and the dielectric constant of the soil-water mixture, κ_m, is defined by:

$$\kappa_m^{\alpha} = 1 + \frac{\rho_b}{\rho_s}(\kappa_{bw}^{\alpha} - 1) + m_v^{\beta}\kappa_{fw}^{\alpha} - m_v \qquad (12)$$

where $\alpha = 0.65$, β is an empirical constant depending on the textural composition of the soil, ρ_b is the bulk density of the soil, κ_{bw} is the density of the solids, κ_{bw} is the bound water dielectric constant, ε_{fw} is the free water dielectric constant and m_v is the volumetric moisture content.

The value of κ_{bw} is given by:

$$\kappa_{bw} = (1.01 + 0.44\,\rho_s)^2 - 0.062 \qquad (13)$$

and κ_{fw} is modeled at a given frequency and temperature using a modified Debye equation, given by:

$$\kappa_{fw} = \kappa_{w\infty} + \frac{\kappa_{wo} - \kappa_{w\infty}}{1 + i2\pi f\tau_w} - i\frac{\rho_{eff}}{2\pi f\kappa_o}\frac{\rho_s - \rho_b}{\rho_s\, m_v} \qquad (14)$$

where $\kappa_{w\infty}$ is the high-frequency limit of κ_w, κ_{wo} is the static dielectric constant of water, τ_w is the relaxation time of water, κ_o is the permittivity of free space equal to 8.854×10^{-12} F.m^{-1}. ρ_{eff} is the effective conductivity, which is an empirically derived function of soil texture, given by:

$$\rho_{eff} = -1.645 + 1.939\,\rho_b - 0.02013\,S + 0.01594\,C \qquad (15)$$

where S and C are percentages of sand and clay.

Modelling of Soil Surface Emissivity

Soil surface emissivity was simulated using the multi-layer radiative transfer model by Wilheit (1978), which calculates the reflectivity of the surface R_o for horizontal and vertical polarizations as a function of wavelength and look angle. It is based on the assumption of coherent radiation (Schmugge and

Choudhury, 1980). The soil is treated as a layered dielectric and the model calculates the dielectric field in each layer. The dielectric field values are used to calculate the energy fluxes and the fractional absorption in each layer denoted f_j^p, where j is the layer and p is the polarization. The brightness temperature is given by:

$$T_B^p = \sum_{j=1}^{N} f_j^p T_j \qquad (16)$$

where T_j denotes the physical temperature of layer j. The fractional absorption in each layer is determined by the vertical distribution of the complex indexes of refraction n_j, which are the square roots of the complex dielectric constants, given by:

$$n_j = \sqrt{\kappa_j' + i\,\kappa_j''}. \qquad (17)$$

where, $\kappa'$and κ'' are the real and imaginary parts of the soil dielectric constant, respectively, as defined by eq. 12. For a semi-infinite medium such as a soil, with no transmission through it, the conservation law of energy yields the reflectivity of the soil:

$$R_o^p = 1 - \sum_{j=1}^{N} f_j^p \qquad (18)$$

In thermal equilibrium, the emissivity equals the absorptivity, and therefore, the emissivity at a certain wavelength λ is given by

$$\varepsilon_s(\lambda) = 1 - R_o^p(\lambda) \qquad (19)$$

Roughness Effects

Roughness reduces the reflectivity and therefore increases the emissivity of the surface. Roughness, however, reduces the sensitivity of emissivity to soil moisture variations and thus reduces the range of the brighness temperature from wet to dry soils (Newton and Rouse, 1980). The increase in emissivity has been modeled empirically by Choudhury et al. (1979) and can be represented by:

$$\Delta\varepsilon = R_o\,(1 - \exp(-h\cos^2\mu)) \qquad (20)$$

where $R_o = 1 - \varepsilon_s$, μ is the look-angle of the radiometer (50° for Nimbus/SMMR) and h is an empirically determined roughness parameter, which is proportional to the RMS height variations of the surface (h = 0 for a smooth surface). The emissivity of the rough bare surface thus equals to:

$$\varepsilon_{sr} = 1 + (\varepsilon_s - 1)\exp(-h') \qquad (21)$$

where the roughness factor h' equals $h\cos^2\mu$.

6.3 The Influence of a Vegetation Canopy

Radiative transfer characteristics of the vegetation are usually expressed in terms of the transmissivity (Γ) or in terms of the optical depth (τ'), with $\Gamma = e^{-(\tau'/\cos\mu)}$. For notation reasons from now on, we will define and use the "oblique" optical depth $\tau=\tau'/\cos\mu$, such that $\Gamma = e^{-\tau}$.

The emitted radiation, expressed in terms of the radiative temperature, T_p, is given for vertical and horizontal polarizations by (Mo et al., 1982):

$$T_p = T_s\,(\varepsilon_{sf(p)})\Gamma_p + (1-\omega_p)T_c(1-\Gamma_p) + \qquad (22)$$

$$+ (1-\varepsilon_{sf(p)})(1-\omega_p)T_c(1-\Gamma_p)\Gamma_p$$

where, ω is the single scattering albedo of the canopy, and T_s and T_c are the temperatures of the soil surface and canopy respectively. For a full cover transparant canopy, with equal soil and foliage temperatures ($T_s = T_c$) eq. 22 reduces to

$$T_p = T_s * [(1 + (1 - \varepsilon_{sf(p)})\Gamma_p)(1-\Gamma_p)(1-\omega_p) + \varepsilon_{sf(p)}\Gamma_p] \qquad (23)$$

The single scattering albedo is generally smaller than 0.1 (Brunfeldt and Ulaby, 1984; Mo et al., 1986; Jackson and O'Neill, 1990) whereas Becker and Choudhury assumed a value of 0.05 for African conditions. The effect on the dynamic range of ε_c from wet to dry soil conditions, however, is small (Owe et al., in press). If the single scattering albedo is assumed to be zero then eq. 23 reduces to

$$T_p = T_s * [1 + (\varepsilon_{sf(p)} - 1)\,(\Gamma^*_p)^2] \qquad (24)$$

where Γ^* is the "effective" transmissivity. The emissivity of a rough vegetation covered surface can be given using eq. 21, in a simplified form, as:

$$\varepsilon_{c(p)} = T_p/T_s = 1 + (\varepsilon_{s(p)} -1)\, e^{-h'}\,(\Gamma^*_p)^2 \qquad (25)$$

6.4 Estimation of $\tau_{6.6}$, τ_{37} and ω

Estimations form Dual Polarized Brightness Temperature

The single scattering albedo and optical depth can be determined using both horizontal and vertical polarized brightness temperatures. Under the assumption that Γ and ω are the same for both polarizations, eq. 23 can be written in a quadratic form for Γ, after elimination of ω, as:

$$a\Gamma^2 + b\Gamma + c = 0 \qquad (26)$$

where $a = R_H - RV$

$b = R_H(1 - T^*_V) - R_V(1 - T^*_H)$

$c = T^*_H - T^*_V$.

Here, T^*_H and T^*_V are the normalized brightness temperatures ($T^*_H = T_H/T_s$, $T^*_V = T_V/T_s$) and R_H and R_V are the surface reflectances ($R_H = 1 - \varepsilon_{s(H)}$, $R_V = 1 - \varepsilon_{s(V)}$). Using the satellite observed brightness temperatures T_V and T_H, and by simulation of R_H and R_V using observed soil moisture profile data, eq. 26 can be solved for Γ whereas ω follows from subsequent substitution of Γ into eq. 23.

Estimation from Horizontal Polarized Brightness Temperatures

If we assume $\omega = 0$ then the "effective" vegetation optical depth, denoted $\tau^*_{(H)}$, follows directly from eq. 25 as:

$$\tau^*_{(H)} = - 1/2 \ln[(\varepsilon_{c(H)} - 1)e^{h'}/(\varepsilon_{s(H)} - 1)] \qquad (27)$$

and thus can be determined directly from the satellite observed normalized brightness temperature ($T_H/T_s \sim \varepsilon_{c(H)}$) and modeled emissivity of the soil, $\varepsilon_{s(H)}$, for any value of the roughness factor h'.

Indices based on Polarization Difference and Ratio

For oblique look-angles, the vegetation optical depth is also related to the difference between horizontal and vertical polarizations. Polarization differences of soil emissivity increase with increasing look angle (Wang et al., 1980). Vegetation, however, tends to saturate the microwave signal in both polarizations with increasing wet biomass (Becker and Choudhury, 1988), especially at higher frequencies, and a high observed polarization difference therefore implies a high transmittance and thus an optically thin vegetation. Assuming that Γ^* and ω are the same for both polarizations and assuming equal soil and canopy temperatures, the polarization difference $\Delta T = T_V - T_H$ can be derived from eq. 22 (Mo et al., 1982), and is given by

$$\Delta T = T_s (R_H - R_V) \Gamma (\Gamma + \omega - \omega \Gamma) \qquad (28)$$

The optical depth τ ($\Gamma = e^{-\tau}$) can now be estimated from this quadratic equation, using the satellite observed polarization difference ΔT, if R_H and R_V are simulated using observed soil moisture profile data. For $\omega = 0$ eq. 28 reduces to:

$$\Delta T = T_s(R_H - R_V) \Gamma^{*2} \qquad (29)$$

Atmospheric scattering and absorption increases with increasing frequency and at 37 GHz the influence on the satellite observed brightness temperature may be substantial (Kerr and Njoku, 1991). Atmospheric influences tend to be reduced in signature ratios rather than in signature differences. The relation between the polarizarion ratio $\xi = T_H/T_V$ and vegetation optical depth can be derived easily from eq. 23 and is given by the quadratic equation:

$$\Gamma^2[(1-\omega)(R_H - \xi R_V)] + \Gamma[\xi\omega(1-R_V) - \omega(1-R_H)] = (1-\omega)(1-\xi) \qquad (30)$$

which gives τ ($\Gamma = e^{-\tau}$) for any values of R_H, R_V, ω and ξ. For $\omega = 0$ eq. 30 reduces to:

$$\Gamma^{*2} = (1-\xi)/(R_H - R_V\xi) \qquad (31)$$

Microwave Polarization Difference Index

The tendency of a vegetation cover to reduce the polarization difference with increasing vegetation biomass was used in several studies to investigate its usefulness for large scale vegetation monitoring (Choudhury et al., 1987; Tucker and Choudhury, 1987) and formed the basis for Becker and Choudhury (1988) to define a microwave based vegetation index at 37 GHz, i.e. the MPDI (Microwave Polarization Difference Index), defined as:

$$MPDI = (20\,\Delta T)/(T_V + T_H) \qquad (32)$$

6.5 Application to Semi-arid Botswana

The remotely sensed data used include 6 GHz (λ = 4.5 cm), 37 GHz (λ = 0.8 cm) microwave horizontally and vertically polarized brightness temperatures from the Scanning Multichannel Microwave Radiometer (SMMR) and 10 day and monthly composites of the Normalized Difference Vegetation Index (NDVI) calculated from visible and near infrared measurements of NOAA/AVHRR.

Profile Soil Moisture

The daily modeled soil moisture refers to the top soil of 10 cm. For modelling the microwave brightness temperature using a multi-layer model, the vertical distribution in the top-layer is important because of the reduced skin depth at the frequencies used here. We modeled the vertical distribution linearly increasing with depth, with an offset of 3 vol.% as visualized in Fig. 14. This offset is based on the fact that even during long periods of drought, the top soil never dried further down. The vertical distribution is thus defined as:

$$\theta(j) = 3 + (1-\alpha)(\theta-3) + \frac{(j-0.5)\alpha(\theta-3)*2}{N} \qquad (33)$$

where $\theta(j)$ is the soil moisture content in vol.% in the j-th layer, θ is the soil moisture content in the 10 cm top soil in vol.%, N is the number of layers (90 according Wilheit's specifications), α is the fraction of the surplus (> 3 vol.%) which is distributed linearly.

6.6 Results and Interpretation

6.6.1 Estimation of Effective Vertical Soil Moisture Distribution

In order to study the effect of different vertical soil moisture distributions and to determine the "large scale effective" distribution we compared the τ^*-values derived form eq. 25 with GAC NDVI-values and with 6.6 GHz optical depths determined from eq. 29 (pol. difference) and eq. 31 (pol. ratio).

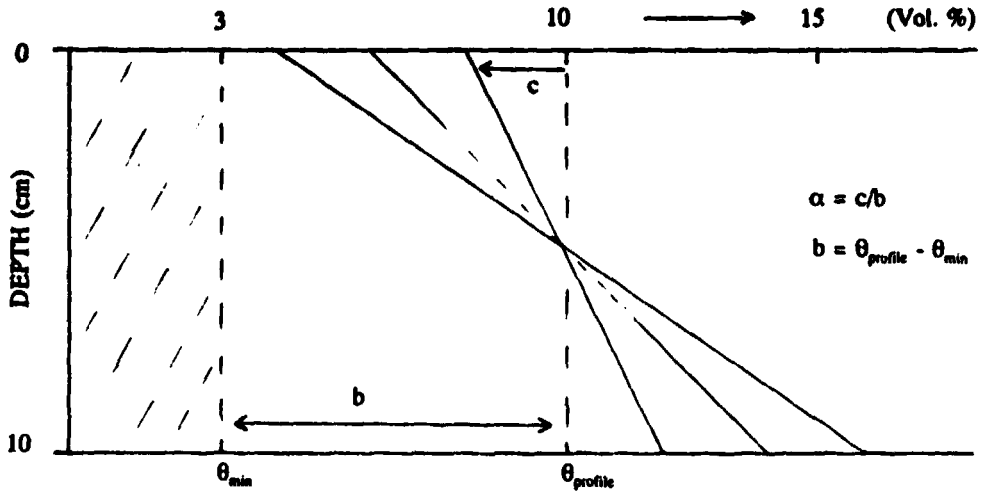

Fig. 14 Simulation of the vertical distribution of top soil moisture. For explanation see text.

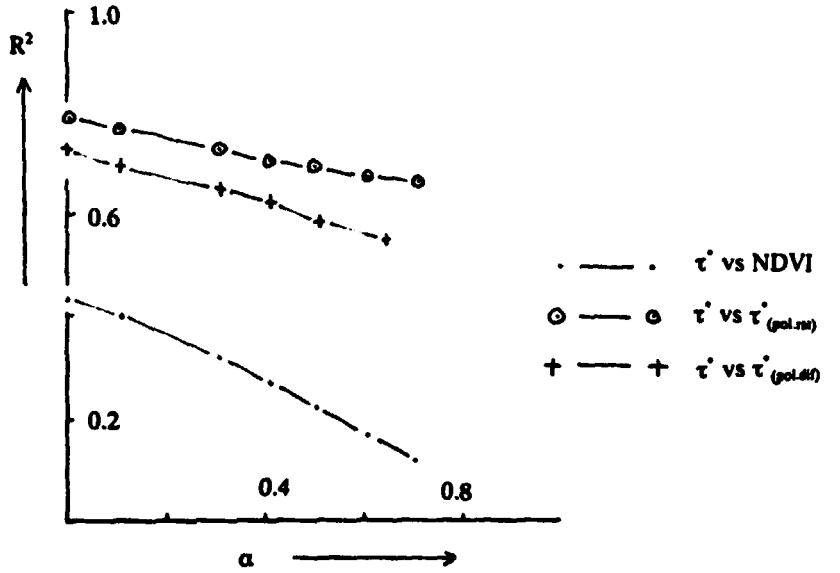

Fig. 15 R^2-values of regression analyses between $\tau^*_{6.6}$ (derived from soil emissivity modeling and satellite observations) and NDVI, $\tau^*_{(pol.dif)}$ and $\tau^*_{(pol.ref)}$ for different values of the soil moisture distribution factor α.

Eqs. 29 and 31 give more or less independent estimates of the 6.6 GHz optical depth based on polarization ratio and polarization difference respectively, which are both almost independent of soil moisture conditions. The τ^*-values were estimated using modeled soil emissivity ε_s and satellite observed brightness temperature. Soil emissivity was modeled for different vertical moisture distributions, i.e. for α = 0.1, 0.2, 0.3, 0.4, 0.5 and 0.9. The results of the comparison are shown in Fig. 15. The highest explained variance occurs with α=0 for all cases, which is probably due to the capability of the top soil to recover to a generally uniform moisture distribution in the top-soil during night time hours. A sensitivity study using different values for the surface roughness indicated that roughness had no influence on the optimum for α = 0. Therefore, we used α = 0 in all further analyses. Since there is no independent way to estimate the roughness parameter we used h = 0.3 which corresponds to a medium rough surface (Choudhury et al., 1979).

6.6.2 Determination of 6.6 and 37 GHz Optical Depths and Single Scattering Albedo's from Satellite Observations

The time series of 6.6 and 37 GHz optical depths (τ) and single scattering albedo's (ω), derived from eqs. 23 and 26, are shown in Fig. 16 (a and b). The albedo at 37 GHz (ω_{37}) turned out to be very stable throughout the 3-year period with an average of 0.096 and a standard deviation of only 0.010. This value fits extremely well within the range ($0.04 < \omega < 0.12$) reported in the literature for cultivated vegetation types.

The albedo at 6.6 GHz ($\omega_{6.6}$) turned out to be less stable throughout the 3-year period, with almost the same average of 0.093 but with a standard deviation of 0.031. The seasonal variations seem to occur during the beginning of the growing season but may very well be due to errors in estimated large scale soil moisture content and thus also due to errors in modeled reflectivity of the soil surface. At 6.6 GHz the transparancy of the vegetation canopy is much higher than at 37 GHz and error propagation in the inverse modeling approach may very well be reflected here.

The optical depths at both frequencies, $\tau_{6.6}$ and τ_{37}, demonstrate the same trend whereas the τ_{37} with an average of approximately 0.9 is much higher than $\tau_{6.6}$ with an average of approximately 0.5. This is in agreement with the theory (Mo et al, 1982; Ulaby et al., 1986). The low extremes ($\tau_{6.6} < 0.4$) at 6.6 GHz are also most probably due to errors in estimated soil moisture. They occur at the beginning of the growing season when optical depths are low and the transparancy is still high. Errors in soil moisture are therefore most strongly propagated during the start of the growing season.

The optical depths, $\tau_{6.6}$ and τ_{37}, demonstrate the same seasonal trends as the NDVI GAC-composites (Fig. 16c), and linear regression analysis showed correlation coefficients of R = 0.80 and R = 0.67, between $\tau_{6.6}$ and NDVI and between τ_{37} and NDVI respectively. Indexes such as NDVI are often used to quantify vegetation characteristics and are generally accepted as a tool to study vegetation trends on various scales (Tucker et al., 1984, 1985). The correlations found between $\tau_{6.6}$, τ_{37} and NDVI support the inverse modeling approach adopted in this study to estimate the microwave effective albedo and optical depths at regional scales.

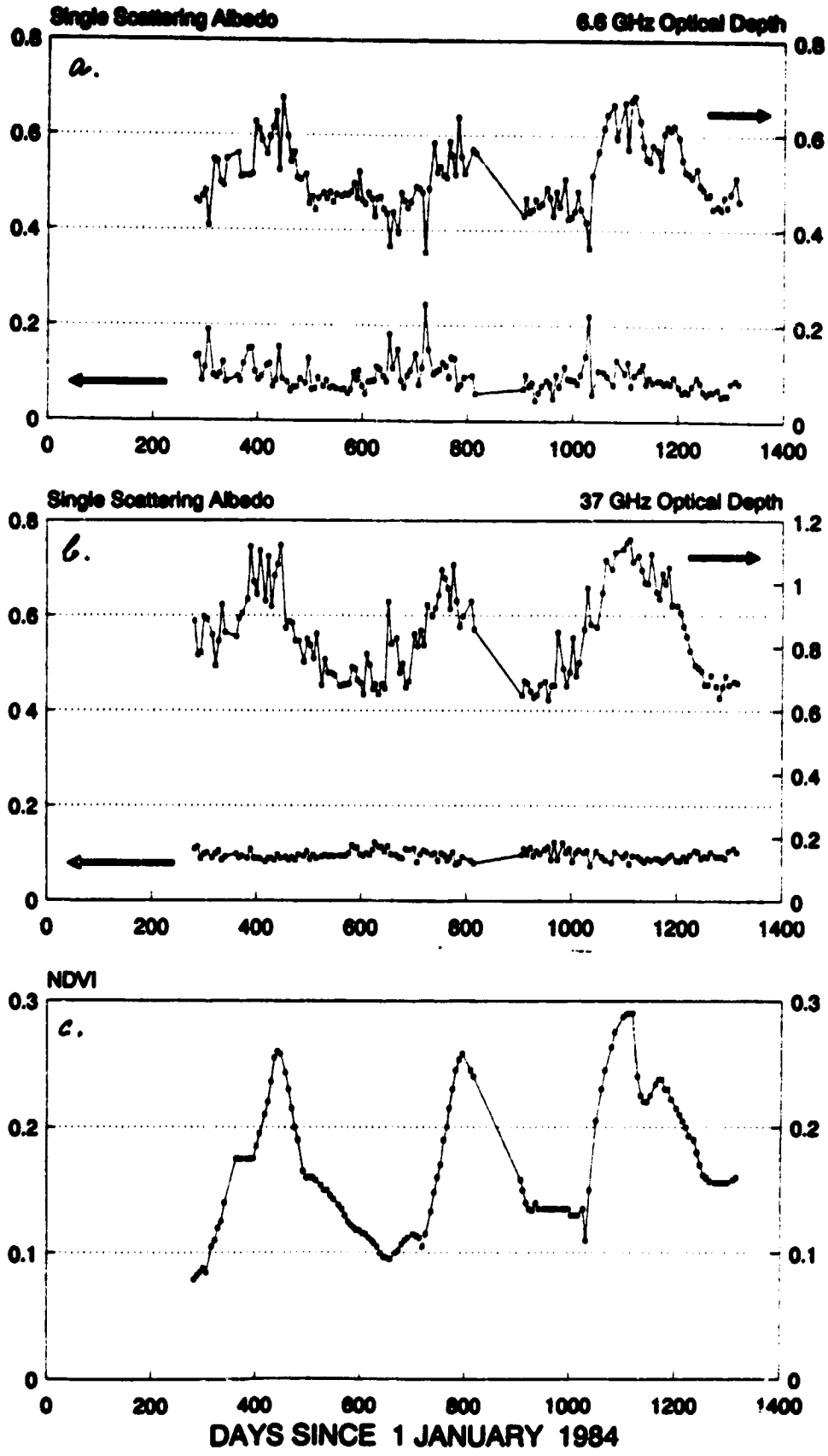

Fig. 16 Time series of 6.6 GHz single scattering albedo and optical depth derived from satellite observed dual polarized brightness temperatures and simulated soil emissivities: 6.6 GHz (a), 37 GHz (b) together with NDVI (c).

6.6.3 Comparison and Analyses of Vegetation Indices and Optical Depth

The NDVI, $\Delta T_{6.6}$, $\xi_{6.6}$, ΔT_{37}, MPDI and ξ_{37} are all indicators of vegetation conditions. NDVI is a measure for the greenness of the vegetation and for green leaf biomass to some extend (Sellers, 1985), whereas the microwave based indices are primarily related to vegetation water content. Although microwave-based signatures of vegetation covered surfaces are influenced by surface soil moisture, this influence is significantly reduced in the pol.difference ΔT. This is because R_H-R_V (eq. 29) is almost independent of soil moisture and relatively constant over the soil moisture range encountered in this study (R_H-R_V = 0.25, with a standard deviation of 0.02). The same counts to some extent for the pol.ratio ξ = T_H/T_V. The influence of soil moisture is theoretically most reduced in the MPDI (eq. 32), where pol.difference is normalized by dividing by the sum of T_V and T_H.

In Fig. 17 the time series of $\Delta T_{6.6}$, ΔT_{37} and NDVI have been plotted together with NDVI and top soil moisture. The time series of $\xi_{6.6}$, ξ_{37} and MPDI have been omitted because they were found to be highly correlated with $\Delta T_{6.6}$ (R^2=0.98), ΔT_{37} (R^2=0.99) and ΔT_{37} (R^2=0.99) respectively. As can be seen, all vegetation indices show basically a comparable annual course (direct or reciprocal) related to the development and senescence of the vegetation. There are, however, very distinct differences in response and variations. Because the optical depth at 37 GHz is much more sensitive to wet biomass variations at low biomass levels than at 6.6 GHz, the variations in $\Delta T_{6.6}$ and ΔT_{37} could well be due to different seasonal regimes between savanna bush and trees on the one hand, and undergrowth of savanna grasses on the other, which together form the major plant associations in south-eastern Botswana. This might then be explained from the differences in physical interaction characteristics of the canopy types. Vegetation is more transparant (lower optical depth) for 6.6 GHz than for 37 GHz radiation which means that grasses have a lower influence on brightness temperatures at 6.6 GHz than at 37 GHz.

Comparison of the time series of $\Delta T_{6.6}$, ΔT_{37} and NDVI on the one hand with soil moisture on the other, however, clearly demonstrates the influence of soil moisture. At 37 GHz, the pol.difference is less influenced by soil moisture due to the lower transmittance of the vegetation (i.e. higher optical depth; τ_{37} = ± 1.0, $\tau_{6.6}$ = ± 0.55). The variations at 37 GHz, superimposed on the annual course, occur during the end of the rainy season and the following dry season due to the fast reaction of grasses on small rainfall events. During these periods $\Delta T_{6.6}$ is extremely invariable (no significant rain; no significant increase in wet biomass). Also at the beginning of the rainy season both indices react in an opposite manner. The 37 GHz displays several dips due to a large storm (fast reaction of grasses and subsequent decrease of ΔT_{37}), whereas 6.6 GHz peaks due to an increase in soil moisture (increase in soil pol.difference and no significant vegetation to compensate for this). The two high peaks in 6.6 GHz are due to soil moisture and are enforced by the absence of significant vegetation. These peaks donot show up in the 37 GHz polarixation difference nor in the MPDI.

Thus, although both 37 GHz and 6.6 GHz polarization difference are potential indicators of the seasonal development of diffferent vegetation associations (grasses on the one hand and bush and trees on the other), the influence of soil moisture dictates a significant part of the fluctuations, especially at 6.6 GHz. The fast response of ΔT_{37} on rainfall events, however, indicates the fast reaction of grasses, and thus the possibility of large scale vegetation monitoring at low biomass levels. This was indicated earlier by Becker and Choudhury (1986).

In Fig. 18 finally, the MPDI is plotted against NDVI. The large scatter, which was also found by becker and Choudhury can be explained to a high extent from the soil moisture influence as explained above. In the same graph also the relation reported by Becker and Choudhury is indicated for comparison.

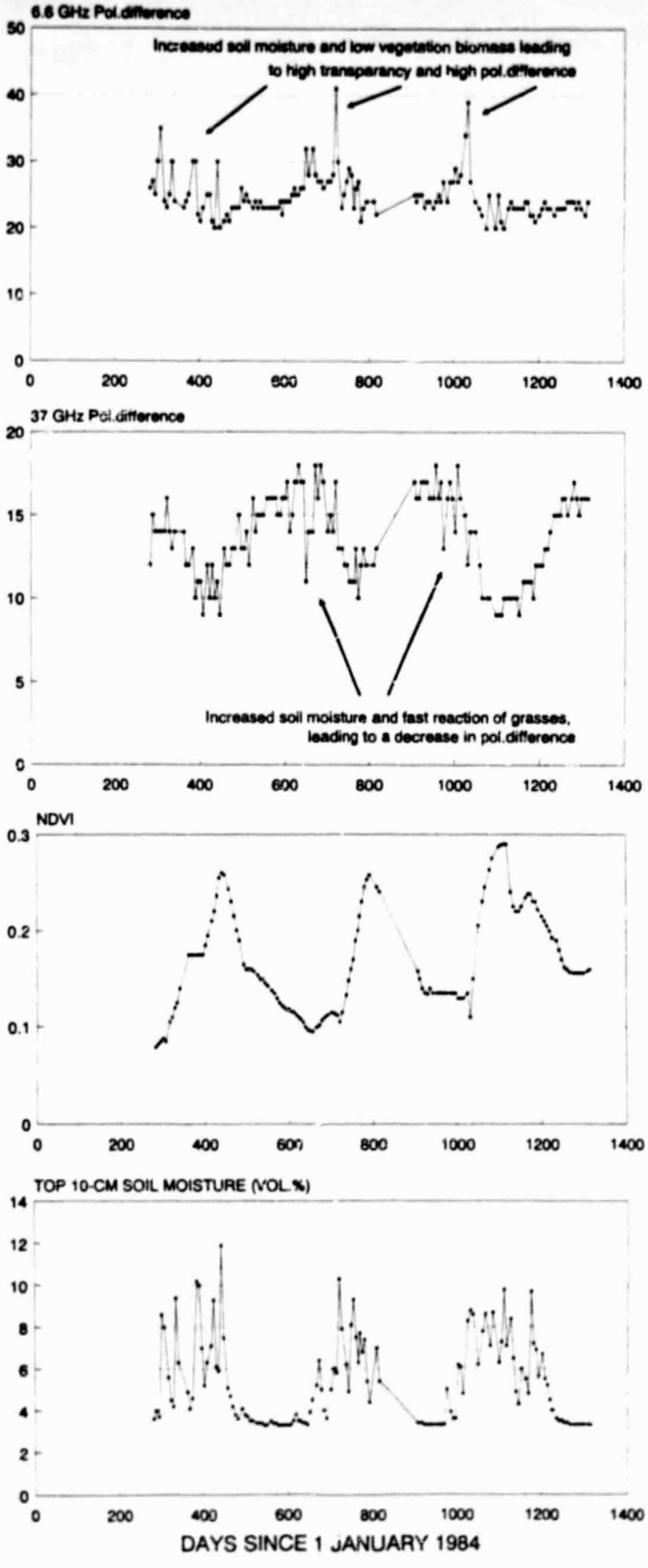

Fig. 17 Time series of vegetation indices $\Delta T_{6.6}$, ΔT_{37} and NDVI, all derived from satellite signatures, and the time series of soil moisture.

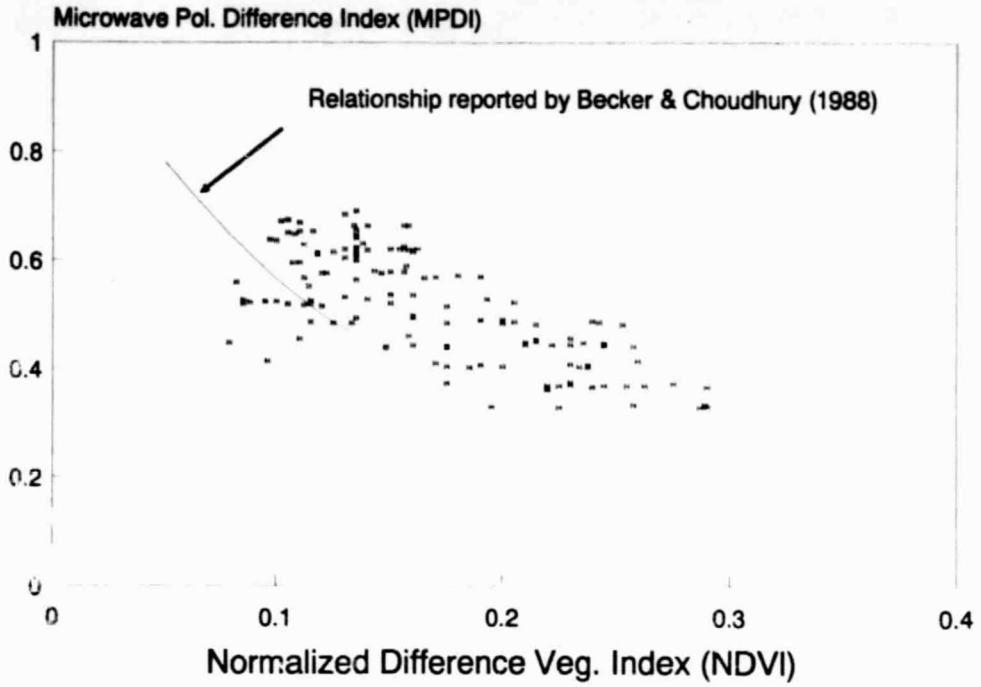

Fig. 18 Scattergram of MPDI versus NDVI. Also the relationship reported by Becker and Choudhury is indicated.

The conclusion by Kerr and Njoku (1991) about the reduced influence of atmospheric conditions on polarization ratio (ξ_{37}) compared to polarization difference (ΔT_{37}) could nor be confirmed in this study. We found both indices extremely high correlated with $R^2 = 0.99$.

6.6.4 Synergetic Approach for Soil Moisture Monitoring

The relationship between large scale soil moisture and normalized brightness temperature for the study area has been studied and described already (Fig. 10) and displays a rather weak relationship with an explained variance (R^2) of 0.45 without correction for vegetation influences. The extraction of soil moisture conditions from satellite microwave brightness temperatures therefore requires a model to simulate the effective emissivity of the complex vegetation covered surface. Inversion of such a model then allows the extraction of soil emissivity from observed brightness temperatures but requires an independent way to estimate the vegetation optical depth to correct for vegetation influences. This leads to a synergetic approach involving different spectral signatures and instruments.

Estimation of $\Gamma_{6.6}$ and $\Gamma^*_{6.6}$ from Satellite Signatures

The transmittances $\Gamma_{6.6}$ and $\Gamma^*_{6.6}$ derived from observed soil moisture and satellite brightness temperatures (using eqs. 26 and 24 respectively) have been compared with the satellite vegetation indices discussed above. In Table 4 the R^2-values for linear regression are given for both transmittances. The R^2-values for

$\Gamma_{6.6}$ are approximately in the same range with the highest correlation for $\Gamma_{6.6}$ = f(NDVI). NDVI is therefore probably the best indicator of vegetation transmittance at 6.6 GHz, followed by MPDI and ΔT_{37} or ξ_{37}, whereas $\Delta T_{6.6}$ and $\xi_{6.6}$ are the worst due to the soil moisture dominance. This is in agreement with conclusions drawn above.

TABLE 4: R^2-values for (non-)linear regression between $\tau_{6.6}$ and $\tau^*_{6.6}$ on the one hand and satellite derived vegetation indices on the other.

R^2	Regression Equation
0.644	$\Gamma_{6.6} = 0.7049 - 0.6141 * NDVI$
0.508	$\Gamma_{6.6} = 0.4522 + 0.2902 * MPDI$
0.497	$\Gamma_{6.6} = 0.4433 + 0.0116 * \Delta T_{37}$
0.512	$\Gamma_{6.6} = 3.5100 - 3.0623 * \xi_{37}$
0.408	$\Gamma_{6.6} = 0.4063 + 0.0079 * \Delta T_{6.6}$
0.416	$\Gamma_{6.6} = 2.4404 - 2.0201 * \xi_{6.6}$
0.440	$\Gamma^*_{6.6} = 0.8094 - 0.5270 * NDVI$
0.133	$\Gamma^*_{6.6} = 0.6416 + 0.1542 * MPDI$
0.138	$\Gamma^*_{6.6} = 0.6343 + 0.0063 * \Delta T_{37}$
0.135	$\Gamma^*_{6.6} = 2.2704 - 1.6311 * \xi_{37}$
0.618	$\Gamma^*_{6.6} = 0.4709 + 0.0101 * \Delta T_{6.6}$
0.620	$\Gamma^*_{6.6} = 3.0517 - 2.5610 * \xi 6.6$

Synergetic Approach based on $\Gamma_{6.6}$ and ω=0.093

The relationships between $\Gamma_{6.6}$, and NDVI and MPDI respectively, are best decribed by (Table 4):

$$\Gamma_{6.6} = 0.7049 - 0.6141 * NDVI \qquad (34)$$

with $R^2 = 0.644$ (Fig. 19a), and by:

$$\Gamma_{6.6} = 0.4522 + 0.2902 * MPDI \qquad (35)$$

with $R^2 = 0.508$.

Using $\Gamma_{6.6}$ = f(NDVI) and inserting this into eq. 24 results in satellite normalized brightness temperatures $T_{H(sim)}$ which correlate with the satellite observed normalized brightness temperatures $T_{H(obs)}$ with $R^2 = 0.69$ ($R = 0.83$). Subsequent inversion of eq. 23, with $\omega = 0.093$, leads to a satellite estimated soil emissivity which correlates with observed soil moisture with $R^2 = 0.642$ (Fig. 19b). Application of $\Gamma_{6.6}$ = f(MPDI) results in an R^2-value between satellite estimated soil emissivity and observed soil moisture of $R^2 = 0.59$ (Fig. 19c). From both applications, $\Gamma_{6.6}$ = f(NDVI) has the highest score. MPDI, however, has the advantage of being cloud independent.

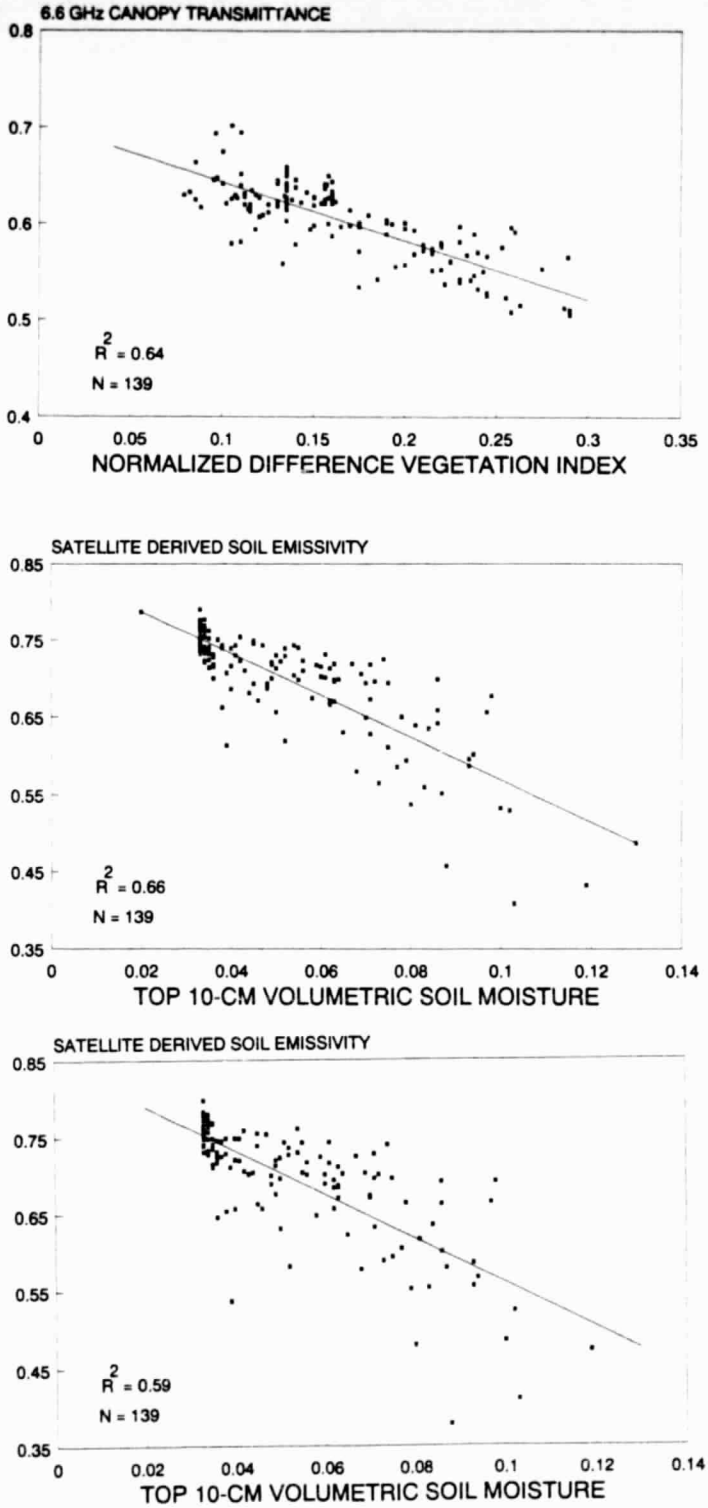

Fig. 19 Simulation results from the synergistic approach with $\Gamma_{6.6}$ and $\omega = 0.093$:

a. Scattergram of $\Gamma_{6.6}$ versus NDVI.

b. Scattergram of satellite derived below canopy soil surface emissivity versus observed top soil moisture, using $\Gamma_{6.6}$ = f(NDVI).

c. Scattergram of satellite derived below canopy soil surface emissivity versus observed top soil moisture, using $\Gamma_{6.6}$ = f(MPDI).

Synergetic Approach based on $\Gamma^*_{6.6}$ and ω=0

Since the single scattering albedo is difficult to estimate without prior knowledge of soil moisture conditions, we also applied a simple, more empirical approach using the effective transmittance $\Gamma^*_{6.6}$, derived from eq. 24, under the assumption that $\omega = 0$.

The R^2-values found for $\Gamma^*_{6.6}$ (Table 4) are much more variable with high and low extremes. For example, $\Gamma^*_{6.6}$ is extremely week correlated with MPDI, ΔT_{37} and ξ_{37}, and strongly correlated with $\Delta T_{6.6}$. The latter relationship is probably an artifact which can be explained from the earlier explained high influence of soil moisture on both $\Delta T_{6.6}$ and the derived $\Gamma^*_{6.6}$.

The relationship between $\Gamma_{6.6}$, and NDVI and MPDI, respectively, is best represented by:

$$\Gamma^*_{6.6} = 0.8094 - 0.5270 * NDVI \qquad (36)$$

with $R^2 = 0.44$ (Fig. 20a).

Using this equation and inserting it into eq. 24 again results in simulated satellite brightness temperature $T_{H(sim)}$ which correlate with the satellite observed brightness temperature $T_{H(obs)}$ with $R^2 = 0.69$. Inversion of eq. 23, with $\omega = 0$, leads to satellite estimated soil emissivities which correlate with observed soil moisture with $R^2 = 0.72$ (Fig. 20b).

The results from both applications ($\Gamma_{6.6}$ and $\Gamma^*_{6.6}$) are comparable, although the use of the effective transmittance $\Gamma^*_{6.6}$ leads to slightly better results. This synergetic approach improves the relationship between satellite observed emissivity and soil moisture from R^2=0.45 (without vegetation correction) to R^2=0.72 (with vegetation correction). The time series of satellite derived soil emissivities and simulated soil emissivities are shown in Fig. 21.

Regarding the large scale and the inherent errors in large scale daily soil moisture estimates, and the non-ideal wavelength at 6.6 GHz for soil moisture studies, the correlations between observed and simulated satellite brightness temperatures and between simulated and derived esoil emissivity are to our opinion extremely high. Since 6.6 GHz penetrates the canopy only partially, the errors are partly due to the fact that vegetation tends to saturate the signal with increasing biomass, whereas a saturated signal with no vegetation indicates a completely dry soil. Thus, a saturated signal may be due to a dry top soil or may result from a full canopy notwithstanding the soil moisture status. The errors in derived soil emissivity therefore partly result from the reduced capability of 6.6 GHz microwaves to fully penetrate canopies with a high level of biomass. Practical application therefore requires an error- and sensitivity analyses to address the achievable accuracy under different vegetation conditions (Ulaby et al., 1983; Theis and Blanchard, 1988). This item is subject of further study.

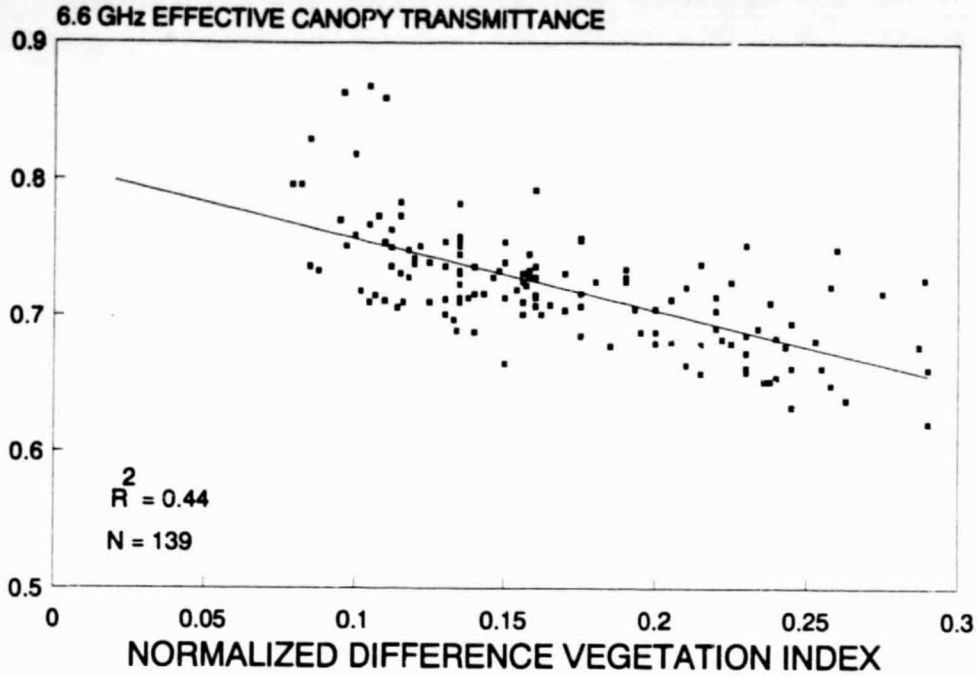

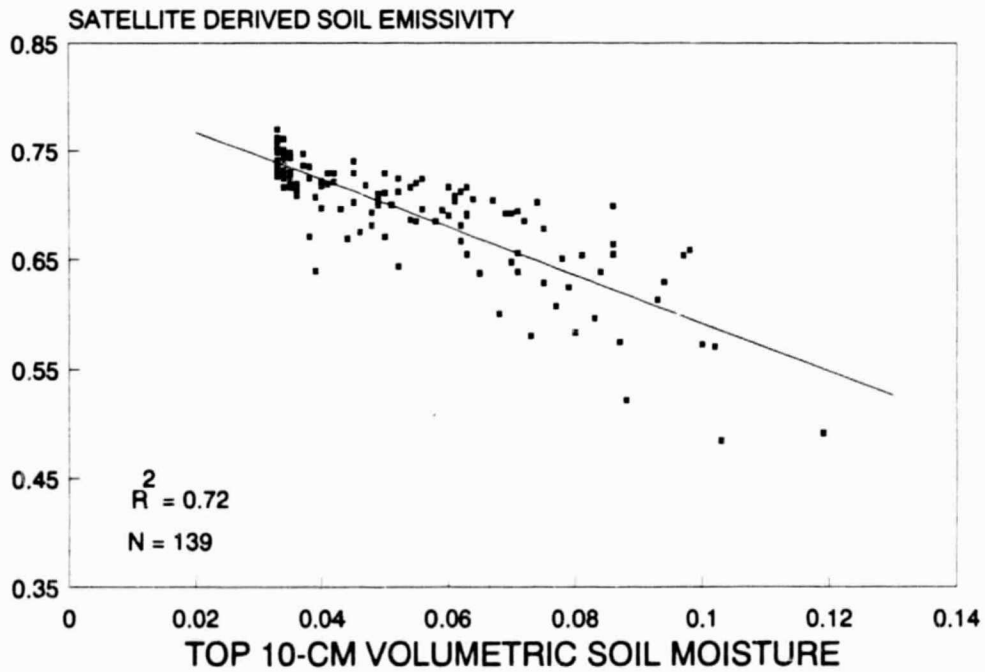

Fig. 20 Simulation results from the synergistic approach with $\Gamma^*_{6.6}$ and $\omega = 0$:

a. Scattergram of $\Gamma^*_{6.6}$ versus NDVI.

b. Scattergram of satellite derived below canopy soil surface emissivity versus observed top soil moisture, using $\Gamma^*_{6.6} = f(\text{NDVI})$.

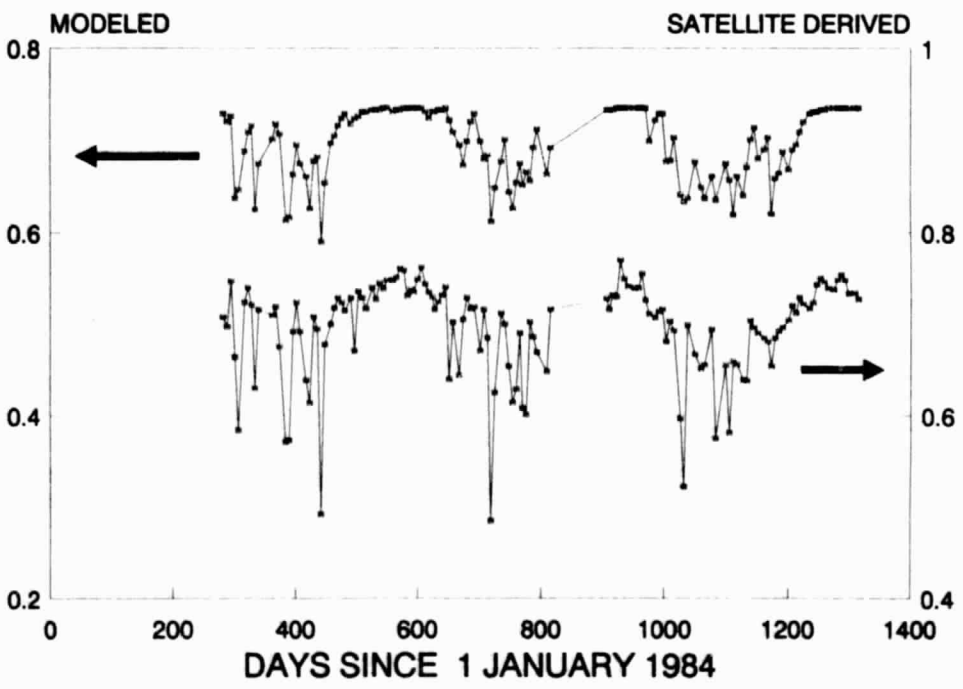

Fig. 21 Time series of satellite derived below canopy soil emissivity (below) and simulated soil emissivity using the radiative transfer model in combination with large scale observed soil moisture.

7 SUMMARY AND CONCLUSIONS

Large scale field measurements of soil moisture were used to calibrate a physically-based daily surface moisture model, and to study the relationship between soil moisture and satellite-derived passive microwave observations. Temperature, solar radiation and rainfall data from 12 precipitation stations permitted the calculation of accurate and spatially representative estimates of surface soil moisture in a 150 km square test site.

The effects of various surface parameters on the emissivity are discussed and demonstrated. Surface roughness is often seen as a noise factor, but at satellite resolutions, the effects may average out when comparing one pixel relative to another. Unless the surface is extremely rough at the field scale, surface roughness may cause little more than a slight offset in the emissivity, especially at the low levels of surface moisture typically seen in a savanna type environment.

Vegetation accounts for much of the variance encountered within the surface moisture data. A canopy, depending on its density, may severely attenuate the natural microwave emission from the surface, while also contributing its own emission to the signal sensed by the satellite radiometer. When sufficiently dense, the canopy will totally mask the radiation emitted from the surface and saturate the signal with its own radiation. The single scattering albedo did not appear to be significant and was set to zero. Transmissivity and optical depth, were shown to have a much greater influence. The NDVI is able to quantify the effects of vegetation to a certain degree, but monthly composite data do not account for variability on shorter time scales, and may not be the optimum parameter for quantifying the variable effects of the vegetation in semi-arid environments.

The use of nighttime brightness temperature data has several demonstrated advantages over daytime acquired data. First, surface moisture is much more evenly distributed throughout the surface profile at night, especially in semi-arid regions where temperature extremes during the day will cause excessive drying of the soil skin layer. Secondly, air temperature is much more closely alligned with surface temperatures (both soil and canopy) at night, and the variability seen during the day due to intermittant canopy cover is less of a factor.

In a follow-up phase, a multi-layer radiative transfer model was used to simulate the large scale emissivity from the soil surface. These simlulated emissivities were used to determine the large scale 6.6 and 37 GHz optical depth and single scattering albedo of the vegetation cover form observed Nimbus/SMMR brightness temperatures. To our knowledge, this study is the first in which actual soil moisture data have been used to derive actual effective optical depths at both microwave frequencies.

The optical depth at 6.6 GHz, $\tau_{6.6}$, is important for estimating soil moisture and to correct for vegetation influences. The optical depth at 37 GHz, τ_{37}, is an indicator of vegetation biomass, only for relatively thin or sparse vegetation covers such as savanna grasses. Both optical depths have been compared with a series of satellite based vegetation indices. It is demonstrated that, although the course of $\Delta T_{6.6}$ and ΔT_{37} each reflect the seasonal dynamics of different vegetation associations (savanna bush and trees on the one hand, and savanna grasses on the other), the signatures and courses are strongly influenced by soil moisture conditions, particularly at the beginning of the wet season when vegetation is still sparse. This is especially true for 6.6 GHz for which we derived a canopy transmittance varying between 0.35 and 0.68. Passive microwave at 37 GHz have some potential for vegetation monitoring, although the influence of soil moisture at low biomass levels, and the tendency of the signal to approach

saturation with increasing biomass form major restrictions.

NDVI was found to be the best indicator of the attenuation effects of the vegetation cover and was used in a synergistic approach to determine the emissivity of the soil surface by inverse modelling, using satellite observed brightness temperatures. Satellite observed brightness temperatures could be simulated with R^2 = 0.69 (R = 0.83), whereas satellite derived soil surface emissivity by inverse modelling was correlated with observed soil moisure with R^2=0.72 (R=0.85). The MPDI, which has the advantage of being an all-weather satellite index, was correlated with the 6.6 GHz optical depth with R^2 = 0.508, and led to an R^2-value between satellite estimated soil emissivity and observed soil mositure of R^2 = 0.58.

Although 6.6 GHz is not an optimum frequency, it has demonstrated considerable potential in quantifying surface moisture in a semi-arid savanna environment, even at low levels of soil moisture. It appeared that the nature of the vegetation in these regions is such that it does interfere significantly with the natural soil emissivity. Using the surface soil moisture data in combination with dual polarization (H and V) microwave signatures led to improved understanding of the influence of typical savanna-type vegetation on the total emissivity. Quantification of these vegetation effects and comparison with NDVI led to a synergistic method of surface soil moisture monitoring using passive microwaves.

The results of the study appear to be promising for the projected Multi-Frequency Imaging Microwave Radiometer (MIMR) with a foot print of 50 km square at 6.6 GHz, planned for the NASA polar platform (EOS-A) within the EOS/Columbus program (ESA, 1990).

REFERENCES

Becker, F. and Choudhury, B.J. (1988): Relative sensitivity of Normalized Difference Vegetation Index (NDVI) and Microwave Polarization Difference Index (MPDI) for vegetation and desertification monitoring. Remote Sensing of Env., Vol. 24: 297-311.

Botswana Ministry of Agriculture (1985): Soil Properties, Crusting and Seedling Emergence. Dryland Farming Research Scheme, Phase III, Vol. 5.

Bruce, J.P. and Clark, R.H. (1966): Introduction to Hydrometeorology. Pergamon Press, Ltd, London, 319 pp.

Brunfeldt, D.R. and Ulaby, F.T. (1984): Measured microwave emission and scattering in vegetation canopies. IEEE Trans. on Geosc. and Remote Sensing, GE-22(6):520-524.

Brutsaert, W.H. (1982): Evaporation into the Atmosphere: Theory, History and Applications. Reidel, Boston, MA, 299pp.

Choudhury, B.J., Schmugge, T.J., Newton, R.W. and Chang, A. (1979): Effect of surface roughness on the microwave emission from soils. J. Geophys. Res., 84: 5699-5706.

Choudhury, B.J., Owe, M., Goward, S.N., Golus, R.E., Ormsby, J.P., Chang, A.T.C. and Wang, J.R. (1987): Quantifying Spatial and Temporal Variations of Microwave Brightness Temperature over the U.S. Southern Great Plains. International Journal of Remote Sensing, 8(2):177-191.

Choudhury, B.J., Idso, S.B. and Reginato, R.J. (1987): Analysis of an Empirical Model for Soil Heat Flux Under a Growing Wheat Crop for Estimating Evaporation by an Infrared Temperature Based Energy Balance Equation. Agricultural and Forest Meteorology, 39:283-297.

Choudhury, B.J. and Tucker, C.J. (1987): Satellite Observed Seasonal and Interannual Variation of Vegetation Over the Kalahari, the Great Victoria Desert, and the Great Sandy Desert:1979-1984. Remote Sensing of Environment, 23:233-241.

Choudhury, B.J., Tucker, C.J., Golus, R.E. and Newcomb, W.W. (1987): Monitoring vegetation using Nimbus-7 scanning multichannel microwave radiometer's data. Int. J. Remote Sensing, Vol. 8 (3): 533-538.

Choudhury, B.J. and Golus, R.E. (1988): Estimating soil wetness using satellite data. Int. J. of Remote Sensing, Vol. 9(7): 1251-1257.

Davies, J.A. and Allen, C.D. (1973): Equilibrium, Potential and Actual Evapotranspiration from Cropped Surfaces in Southern Ontario. Journal of Applied Meteorology, 12:649.

De Bruin, H.A.R. (1983): A Model for the Priestley-Taylor Parameter Alpha. Journal of Climate and Applied Meteorology, 22:572-578.

Dobson, M.C., Ulaby, F.T. Hallikainen, M.T. and El-Rayes, M.A. (1985): Microwave Dielectric Behavior

of Wet Soil - Part II: Dielectric Mixing Models. IEEE Trans. on geosc. and Remote Sensing, Vol. GE-23 (1): 35-46.

El-Rayes, M.A. and Ulaby, F.T. (1987): Microwave Dielectric Spectrum of Vegetation - Part I: Experimental Observations. IEEE Trans. Geosc. and R.S., Vol. GE-25(5): 541-549.

ESA-European Space Agency (1990): The Multi-Frequency Imaging Microwave Radiometer. Instrument Panel report, ESA-SP-1138.

Fung, A.K. and Eom, H.Y. (1985): A Comparison Between Active and Passive Sensing of Soil Moisture from Vegetated Terrains. IEEE Transactions on Geoscience and Remote Sensing, GE-23(5):768-775.

Jackson, T.J., Schmugge, T.J. and O'Neill, P. (1984): Passive microwave remote sensing of soil moisture from a aircraft platform. Remote Sensing of Environment, 14: 135-151.

Jackson, T.J. and O'Neill, P.E. (1990): Attenuation of soil microwave emission by corn and soybeans at 1.4 and 5 GHz. IEEE Trans. on Geosc. and Remote Sensing, 28(50), 978-980.

Jackson, T.J., Schmugge, T.J. and Wang, J.R. (1982): Passive Microwave Sensing of Soil moisture under Vegetation Canopies. Water Res. Res., Vol. 18(4): 1137-1142.

Kerr, Y.H. and Njoku, E.G. (1991): On the use of passive microwaves at 37 GHz. Int. Colloquium Physical measurements and Signatures in remote sensing. January, 14-18, 1991, Courchevel, France.

Kennedy, P.J. (1989): Monitoring the phenology of Tunisian grazing lands. Int. J. of R.S., Vol. 10(4/5): 835-845.

Kirdiashev, A.A., Chukhlantsev, C.B. and Shutko, A.M. (1979): Microwave Radiation of the Earth's Surface in the Presence of Vegetation Cover. Radio Engineering Electronics, 24:256-264.

Mo, T., Choudhury, B.J., Schmugge, T.J. and Jackson, T.J. (1982): A model for microwave emission from vegetation-covered fields. J. Geophys. Res., Vol. 87: 11229-11237.

Newton, R.W. and Rouse, J.W. (1980): Microwave radiometer measurements of moisture content. IEEE Trans. Antennas Propagation, AP-28: 680-686.

Owe, M., Chang, A. and Golus, R.E. (1988): Estimating Surface Soil Moisture from Satellite Microwave measurements and a Satellite Derived Vegetation Index. Remote Sensing of Environm., Vol. 24: 331-345.

Owe, M. and Van de Griend, A.A. (1991): A Daily Surface Moisture Model for Large Area Semi-Arid Land Application with Limited Climate Data. Journal of Hydrology, Vol. 121:119-132.

Owe, M., Van de Griend, A.A. and Chang, A.T.C. (1992): Surface Soil Moisture and Satellite Passive Microwave Observations in Semi-Arid Southern Africa, Water Resources Research (in press).

Pampaloni, P. and Paloscia, S. (1986): Microwave Emission and Plant Water Content: A Comparison

Between Field Measurements and Theory. IEEE Transactions Geoscience and Remote Sensing, GE-24:900-905.

Pitts, D.E., Badhwar, G.D., Reyna, E., Zoughi, R., Wu, L.K. and Moore, R.K. (1988): Estimation of X-Band Scattering Properties of Tree Components. IEEE Transactions Geoscience Remote Sensing, Vol. 26(5):612-616.

Priestley, C.H.B. and Taylor, R.J. (1972): On the Assessment of Surface Heat Flux and Evaportation Using Large-Scale Parameters. Monthly Weather Review, 100:81-92.

Ringrose, S. and Matheson, W. (1987): Spectral Assessment of Range Degradation in the Botswana Hardveld Environment. Remote Sensing of Environment, Vol. 23:379-396.

Ringrose, S., Matheson, W., Mogosi, B. and Tempest, F. (1990): The Darkening Effect in Drought Affected Savanna Woodland Environment Relative to Soil Reflectance in the LANDSAT and SPOT Wavebands. Remote Sensing of Environment (in press).

Ringrose, S., Matheson, W., Tempest, F. and Boyle, T. (1990): The Development and Causes of Range Degradation Features in Southeast Botswana Using Multi-Temporal LANDSAT MSS Imagery. Photogrammetric Engineering and Remote Sensing, Vol. 56(9):1253-1262.

Sellers, P.J. (1985): Canopy reflectance, photosynthesis and transpiration. Int. J. Remote Sensing (6):1335-1372.

Siderius, W. (1973): Soil Transitions in Central East Botswana (Africa). Krips Repro Meppel, The Netherlands, 260 pp.

Schmugge, T. (1985): Remote Sensing of Soil Moisture. In: Hydrological Forecasting, M.G. Anderson and T.P. Burt (Eds.), John Wiley & Sons, Ch. 3:37-76.

Schmugge, T.J., O'Neill, P.E. and Wang, J.R. (1986): Passive Microwave Soil Moisture Research. IEEE Trans. on Geoscience and Remote Sensing, Vol. GE-24(1):12-22.

Schmugge, T.J. and Choudhury, B.J. (1980): A comparison of radiative transfer models for predicting the microwave emission from soils. NASA-Techn. Memorandum 80688, May, 1980, GSFC Greenbelt, MD 20771 (USA).

Theis, S.W., Blanchard, B.J. and Newton, R.W. (1984): Utilization of Vegetation Indices to Improve Microwave Soil Moisture Estimates Over Agricultural Lands. IEEE Transactions Geoscience Remote Sensing GE-22(6):490-495.

Theis, S.W., Blanchard, B.J. and Blanchard, A.J. (1986): Utilization of Active Microwave Roughness Measurements to Improve Passive Microwave Soil Moisture Estimates Over Bare Soils. IEEE Transactions Geoscience Remote Sensing, GE-24:334-339.

Theis, S.W. and Blanchard, A.J. (1988): The effect of measurement error and confusion from vegetation on passive microwave estimates of soil moisture. Int. J. of Remote Sensing, Vol. 9(2): 333-340.

Tucker, C.J., Van Praet, C, Boerwinkel, E. and Gaston, A. (1983): Satellite Remote Sensing of Total Dry Matter Production in the Senegalese Sahel. Remote Sensing of Environment 13: 461 - 474.

Tucker, C.J., Gatlin, J.A. and Schneider, S.R. (1984): Monitoring Vegetation in the Nile Delta with NOAA-6 and NOAA-7 AVHRR Imagery. Photogrammetric Engineering and Remote Sensing, 50(1):53-61.

Tucker, C.J., Vanpraet, C.L., Sharman, M.J. and Ittersum, G. (1985): Satellite Remote Sensing of Total Herbaceous Biomass Production in the Senegalese Sahel: 1980-1984. Remote Sensing of Environment, 17:233-249.

Ulaby, F.T., Razani, M. and Dobson, M.C. (1983): Effects of vegetation cover on the microwave radiometric sensitivity of soil moisture. IEEE Trans. on Geoscience and Remote Sensing, Vol. GE-21(1): 51-61.

Ulaby, F.T., Moore, R.K. and Fung, A.K. (1986): Microwave Remote Sensing - Active and Passive. Vol. III: From Theory to Applications. Chapter 19, p. 1551 a.f.

Ulaby, F.T. and El-Rayes, M.A. (1987): Dielectric Spectrum of Vegetation - Part II: Dual-Dispersion Model. IEEE Trans. Geosc. and R.S., Vol. GE-25(5): 550-557.

Van de Griend, A.A., Owe, M. and Carter, D.C. (1990): Microwave remote sensing of soil moisture in Africa using Nimbus-7/SMMR. Proc. Int. Symp. "Remote Sensing and Water Resources", Enschede (NL), August 20-24, 1990:277-285.

Wang, J.R. (1983): Passive Microwave Sensing of Soil Moisture Content: The Effects of Soil Bulk Density and Surface Roughness. Remote Sensing of Environment, 13:329-344.

Wang, J.R. (1985): Effect of vegetation on soil moisture sensing observed from orbiting microwave radiometers. Remote Sensing of Env., Vol. 17: 141-151.

Wang, J.R. and Schmugge, T.J. (1980): An Empirical Model for the Complex Dielectric Permittivity of Soils as a Function of Water Content. IEEE Transactions Geoscience and Remote Sensing, GE-18(4):288-295.

Wang, J.R., Newton, R.W. and Rouse, J.W. (1980): Passive microwave remote sensing of soil moisture: The effect of tilled row structure. IEEE Trans. Geosc. and Remote Sensing, GE-18: 296-302.

Wang, J.R., McMurtrey, J.E., Engman, E.T., Jackson, T.J., Schmugge, T.J., Gould, W.I., Fuchs, J.E. and Glazer, W.S. (1982): Radiometric Measurements Over Bare and Vegetated Fields at 1.4 GHz and 5 GHz Frequencies. Remote Sensing of Environment, 12:295-311.

Wilheit, T.T. (1978): Radiative Transfer in a Plane Stratisfied Dielectric. IEEE Trans. on Geosc. and Electr. Vol. 2, GE-16: 138-143.

ACKNOWLEDGEMENTS

The Botswana Water and Surface Energy Balance Research Program has been made possible by grants and material support from the Netherlands Remote Sensing Board (BCRS) (NL), Project AO-4.4; NASA Headquarters, Code SEL (U.S.A.); the Vrije Universiteit of Amsterdam (Faculty of Earth Sciences); and the Remote Sensing Unit of FAO in Rome (Italy). We wish to thank Mrs. G.K. Ramothwa (director), Dr. P. Vossen (now with JRC/ISPRA, Italy), and Mr. K.R. Tsele, all of the Meteorological Service of Botswana for their continuous support. Thanks are also due to Prof. Dr. R.J. Gurney (NERC/University of Reading, former head of the Hydrological Sciences Branch (NASA/GSFC), Dr. E.T. Engman (Head Hydrological Sciences Branch (NASA/GSFC) for their encouraging support and to Dr. D.C. Carter (USAID/INTSORMIL, Kansas State University). The NOAA/AVHRR data was graciously supplied by Dr. C.J. Tucker of the Goddard GIMMS Group (NASA/GSFC).

ANNEX 1: OVERVIEW OF SCIENTIFIC PUBLICATIONS RESULTING FROM BOTSWANA-1 (Journals, Conference Proceedings and Abstracts)

JOURNALS

Owe, M. and Van de Griend, A.A. (1990): Daily surface moisture model for large scale semi-arid land application with limited climate data. Journal of Hydrology, Vol. 121:119-132.

Owe, M., Van de Griend, A.A. and Chang, A.T.C. (1992): Surface moisture and satellite microwave observations in semi-arid southern Africa. Water Resources Research (in press).

Owe, M., Van de Griend, A.A. and Carter, D.C. (submitted): Modeliing of longterm surface soil moisture and monitoring of vegetation biomass response by satellite in semi-arid Botswana. Submitted to: Journal of Hydrological Processes.

Van de Griend, A.A., Owe, M., Vugts, H.F. and Prince, S.D. (1989): Water and energy balance modelling in Botswana. Bull. of the American Meteorological Society, Vol. 70(11): 1404-1411.

Van de Griend, A.A., Owe, M., Groen, M. and Stoll, M.Ph. (1991): Measurement and spatial variation of thermal infrared surface emissivity in a savanna environment. Water Resources Research, Vol. 27 (3):371-379.

Van de Griend, A.A. and Owe, M. (1992): On the relationship between thermal emissivity and the Normalized Difference Vegetation Index for natural surfaces. Int. Journal of Remote Sensing (In Press).

Van de Griend, A.A. and Owe, M. (submitted): Determination of microwave vegetation optical depth and single scattering albedo from large scale soil moisture and Nimbus/SMMR satellite observations. Submitted to: Int. Journal of Remote Sensing.

Van de Griend, A.A. and Owe, M. (submitted): Microwave vegetation optical depth and inverse modeling of soil emissivity using Nimbus/SMMR satellite observations. Submitted to: J. of Geophysical Research.

Van de Griend, A.A. and Owe, M. (in review at NASA/GSFC): The estimation of atmospheric turbidity using NOAA/AVHRR: Theoretical approach and simulation results.

CONFERENCE PROCEEDINGS

Van de Griend, A.A., Owe, M., Vugts, H.F., Prince, S.D., Tesselaar, F.W. and De Bruin, H.A.R. (1990): Collection of ground data for pixel scale parameterization of energy balance models for remote sensing purposes. In: Proc. Int. Symposium IGARSS'90 "Remote Sensing Science for the Nineties", Washington, D.C. (USA), May 20-24: 1251-1256.

Van de Griend, A.A., Owe, M. and Carter, D.C. (1990): Microwave remote sensing of soil moisture in Africa using Nimbus-7/SMMR. Proc. Int. Symp. "Remote Sensing and Water Resources", Enschede (NL), August 20-24, 1990:277-285.

ABSTRACTS

"Water and Energy Balance Modelling in Botswana", A.A. van de Griend, M. Owe and H.F. Vugts, Abstract in EOS p. 347, presented at American Geophysical Union Spring Meeting, Baltimore, Md (USA).

"Satellite Monitoring of Soil Moisture in Semi-Arid Southern Africa", M. Owe, H. van Elburg and A.A. van de Griend. Abstract in EOS, p. 347, presented at American Geophysical Union Spring meeting, Baltimore, Md (USA).

"A Cable System for Mesuring Thermal Infrared Surface Temperatures", A.A. van de Griend and M. Owe, presented at American Society of Agronomy, Symposium on Biophysical Measurement, Agronomy Abstracts. Las Vegas, Nv (USA).

"A Simple Device for the Measurement of Thermal Infrared Surface Emissivity", M. Owe and A.A. van de Griend, 81st Annual Meeting, American Society of Agronomy, Symposium on remote Sensing of Plants and Soil. Agronomy Abstracts. Las Vegas, Nv (USA).